Modelling, Analysis, and Simulation of Mobile-To-Mobile MIMO Channels

by

Nattaporn Sahadech

Thesis in partial fulfilment of the degree of
Master in Technology in
Information and Communication Technology

Agder University College
Faculty of Engineering and Science

Grimstad
Norway

May 2006

Contents

Symbols

$<$	less than
$=$	equal
$\approx$	approximately equal
$\leq$	less than or equal to
$(a, b]$	set of numbers within the left hand side open interval from a to b
$[a, b]$	set of numbers within the closed interval from a to b
$\mid a \mid$	absolute value of a
$\sqrt{a}$	principal value of the square root of a, i.e., $\sqrt{a} \geq 0$ für $x \geq 0$
$a \rightarrow b$	a tends to b or a approaches b
$b = \frac{a}{c} = a/c$	quotient of a and c
$b = ac = a \cdot c = a \times c$	product of a and c
$b = \int_a^c x(t)dt$	integral of the function $x(t)$ over the in interval $[a, c]$
$b = \sum_{i=0}^{n} a_i$	sum of n summands
$b = a \pm c$	sum and difference of a and c
$E\{x\}$	mean value or expected value of x
e^x	exponential function
$F(x)$	cumulative distribution function
$F^{-1}(x)$	inverse cumulative distribution function
$Im\{x\}$	imaginary part of $x = x_1 + jx_2$

$Re\{x\}$	real part of $x = x_1 + jx_2$
x^*	complex conjugate of the complex number $x = x_1 + jx_2$
$\mathcal{F}\{x\}$	Fourier transform of $X(f)$
$\mathcal{F}^{-1}\{x\}$	inverse Fourier transform of $X(f)$
$\ddot{x}(t) = \frac{d^2x}{d^2t}$	second derivative of the function $x(t)$ with respect to t
$\dot{x}(t) = \frac{dx}{dt}$	derivative of the function $x(t)$ with respect to t
$\tilde{a}_l$	delay coefficient of the lth path
A_R	antenna element of the receiver
A_T	antenna element of the transmitter
B_c	coherence bandwidth
B_s	bandwidth of a signal
$B_{\mu\mu}^{(1)}$	mean Doppler shift
$B_{\mu\mu}^{(2)}$	Doppler spread
c	the speed of light
c_n	Doppler coefficient of the nth component
$c_{n,l}$	Doppler coefficient of the nth component of the lth path
D	distance between mobile stations
$E_{r_{\mu\mu}}$	mean-square error of the autocorrelation function
f	Doppler frequency
f_n	Doppler frequency of the nth component
f_0	carrier frequency
$F_\zeta(r)$	cumulative distribution function of a Rayleigh process
f_l	lower frequency
$f_{n,l}$	Doppler frequency of the nth component of the lth path
$f_{R_{\max}}$	maximum Doppler frequency caused by the motion of the receiver
f_R	Doppler frequency of the receiver

$f_{T_{\max}}$	maximum Doppler frequency caused by the motion of the transmitter
f_T	Doppler frequency of the transmitter
f_u	upper frequency
h	half of the street width
$h(\tau', t)$	time-variant channel impulse response
$H(f', t)$	time-variant channel transfer function
$h_{ij}(t)$	diffuse component between jth transmit and ith receive antenna
l	length of a cluster, e.g., building width
l_c	length of the cth cluster
N	number of exponential functions (scattered components)
$N(r)$	level-crossing rate
n_R	number of receive antennas
n_T	number of transmit antennas
$N_\zeta(r)$	level-crossing rate of a Rayleigh process
$p_{\Delta\alpha}(\Delta\alpha)$	probability density function of the angle of spreading $\Delta\alpha$
$p_{\Delta\theta}(\Delta\theta)$	probability density function of the angle of spreading $\Delta\theta$
$p_f(f)$	probability density function of the Doppler frequency
r	amplitude level
$r_{\mu\mu}(\tau)$	autocorrelation function
$r_{\mu_1\mu_2}(\tau)$	cross-correlation function
$r_{\tau'\tau'}(\upsilon')$	frequency correlation function
$r_{hh}(\cdot, \cdot; \cdot, \cdot)$	autocorrelation function of $h(\tau', t)$
$S(\tau', f)$	scattering function of a frequency-selective stochastic process
$s(\tau', f)$	Doppler-variant impulse response
$S_{\mu\mu}(f)$	Doppler power spectral density function

$S_{\tau'\tau'}(\tau')$	delay power spectral density
t	time variable
$T(f', f)$	Doppler-variant transfer function
$T_\zeta(r)$	average duration of fades of a Rayleigh process
v_R	speed of the receiver
v_T	speed of the transmitter
w_c	weighting factor for the cth cluster of scatterers
$x(t)$	input signal
$y(t)$	output signal
$\mathcal{C}$	number of clusters
$\mathcal{L}$	number of discrete paths
$\hat{\mu}(t)$	stochastic process
$\hat{r}_{\mu\mu}(\tau)$	autocorrelation function of the stochastic simulation model
$\mu(t)$	zero-mean complex Gaussian random process
$\tilde{\mu}(t)$	deterministic process
$\tilde{\mu}_l(t)$	deterministic process of the lth path
$\tilde{B}^{(1)}_{\mu\mu}$	mean Doppler shift of a deterministic process
$\tilde{B}^{(2)}_{\mu\mu}$	Doppler spread of a deterministic process
$\tilde{h}(\tau', t)$	time-variant impulse response of the deterministic simulation model
$\tilde{r}_{\mu\mu}(\tau)$	autocorrelation function of the deterministic simulation model
$\tilde{r}_{\tau'\tau'}(\upsilon')$	frequency correlation function of a deterministic process
$\tilde{S}(\tau', f)$	scattering function of a frequency-selective deterministic process
$\tilde{S}_{\tau'\tau'}(\tau')$	delay power spectral density of a deterministic process
α	angle of departure
α_0	initial angle of departure
α_b	boundary angle of departure

α_c	critical angle of departure
α_v	angle of direction of motion of the transmitter
β	negative curvature of the autocorrelation function at the origin, i.e., $\beta = \ddot{r}_{\mu\mu}(0)$
$\Delta\alpha$	angle of spreading at the transmitter
$\Delta\alpha_{\max}$	maximum angle of spreading at the transmitter
$\Delta\theta$	angle of spreading at the receiver
$\Delta\theta_{\max}$	maximum angle of spreading at the receiver
δ_R	space between antennas at the receiver
δ_T	space between antennas at the transmitter
λ	wavelength
Φ_0	cross-correlation function at $\tau = 0$
Ψ_0	autocorrelation function at $\tau = 0$
σ_0^2	mean power
τ	time difference between t_2 and t_1, i.e., $\tau = t_2 - t_1$
τ'	continuous propagation delay
τ_l'	discrete propagation delay of the lth path
$\tau_{\max}$	maximum propagation delay
θ	angle of arrival
θ_0	initial angle of arrival
θ_b	boundary angle of arrival
θ_c	critical angle of arrival
θ_n	Doppler phase of the nth component
θ_v	angle of direction of motion of the receiver
$\theta_{n,l}$	Doppler phase of the nth component of the lth path
$\tilde{\tau}_l'$	discrete propagation delay of the lth path of a deterministic process

Abbreviations

ACF	autocorrelation function
ADF	average duration of fades
AOA	angle of arrival
AOD	angle of departure
CCF	cross-correlation function
CDF	cumulative distribution function
COST	European Cooperation in the Field of Scientific and Technical Research
D-AMPS	Digital American Mobile Phone System
DECT	Digital European Cordless Telephone
FCF	frequency correlation function
GBSBM	geometrical based single bounce model
GSM	Global System for Mobile Communications
INMARSAT	International Maritime Satellite Organization
LCR	level-crossing rate
LPNM	L_p-norm method
MBS	Mobile Broadband Systems
MIMO	multiple-input multiple-output
PDC	Personal Digital Cellular
PDF	probability density function
PSD	Doppler power spectral density function
SISO	single-input single-output
TETRA	Trans European Trunked Radio Access
UMTS	Universal Mobile Telecommunications Systems
WGN	white Gaussian noise
WLAN	Wireless Local Area Networks
WSSUS	wide-sense stationary uncorrelated scattering

List of Figures

Abstract

The development of mobile communication has been dramatically increasing in recent years. New concepts and methods are necessary for the improvement of existing mobile communication techniques due to the fact of the demand for these systems with higher data rates and a better quality of service. As the number of subscribers is growing rapidly, the development of mobile radio channel models has become one of the most important research topics within mobile communication systems.

This thesis deals with a multiple-input multiple-output (MIMO) channel model for mobile-to-mobile communications. It starts with an analysis of a single-input single-output (SISO) channel model which is based on a geometrical street model under the assumption that the transmitter and the receiver are moving. Starting from the geometrical model, statistical properties of the analytical and simulation models will be studied. Of special interest are the probability density function, temporal autocorrelation function, Doppler power spectral density, level-crossing rate, and average duration of fades. Furthermore, the analytical results will be verified by MATLAB simulations. In the last part of this thesis the extensions of the SISO street model with respect to multiple clusters of scatterers, frequency selectivity, and to a MIMO street model are considered.

Keywords: Mobile fading channels, mobile-to-mobile channels, SISO channels, MIMO channels.

Acknowledgment

This thesis was carried out during my exchange semester at Agder University College from January to May 2006. This work is my additional master's thesis in information and communication technology. I hereby confirm that I have composed this completed work independently and no one else involved except the specified sources and quotations.

Since communication plays an important role of everyday life, in relation to this thesis, I am deeply thankful for the communication with my supervisor Prof. Matthias Pätzold at Agder University College for his competent support during this work. Furthermore, I am also grateful to Mr. Bjørn Olav Hogstad for his help with the simulation using MATLAB. I would also like to thank Mr. Stein Bergsmark, the head of study at Agder University College, for his counsel during this thesis.

Nattaporn Sahadech
Grimstad, May 2006.

Chapter 1

Introduction

1.1 The Development of Mobile Communication Systems

Mobile communication systems have become an important part of everyday life and are well known allover the world due to the fact that they help people and machines to communicate in any manner, such as data, voice, image or video. Because of their rapidly growing use and successful development in recent years, mobile communication is one of the most interesting subjects for many engineers and scientists, therefore, the research and development of this field will increase over the next years.

In the past, different kinds of mobile radio systems for various applications, such as aviation and navigation oversea by INMARSAT (International Maritime Satellite Organization), national long-distance call with C-net, and wireless telephone for the home area with CT1+ have been developed. These systems are referred to as the first generation of mobile systems, which were used primarily only for analog transmission technology with the limitation of communication possibilities.

The second generation (2G) is characterized by digital signal transmission. The modification from analog to digital was driven by its higher capacity and the improved cost, speed, and power efficiency of digital hardware [21]. Examples of 2G technologies are GSM (Global System for Mobile Communications), DECT (Digital European Cordless Telephone), PDC (Personal Digital Cellular), D-AMPS (Digital American Mobile Phone System), and TETRA (Trans European Trunked Radio Access).

The third generation mobile systems (3G) are driven by the need for high-speed data transmission capabilities while on the move. The three evolving networks in Europe are UMTS (Universal Mobile Telecommunications Systems), MBS (Mobile Broadband Sys-

tems), and WLAN (Wireless Local Area Networks). The 3G standard UMTS is an upgrade of the GSM. The challenge for the third generation of mobile radio systems is to transmit large quantities of data. With substantially enhanced capacity, quality, and data rates, 3G technology provides customers with high-speed access anytime and anywhere. The radio channel has significant effects on the capacity and transmission properties of mobile communication systems.

1.2 Mobile Radio Channels

The path between transmitter and receiver is often obstructed by several natural and man-made structures. The presence of these obstacles on the received signal manifests itself in several ways, such as additional path loss, distortion, and spreading of the received signal, etc. By the radio wave propagation is generally meant the movement of electromagnetic waves from a transmitting antenna to a receiving antenna in the presence of one or more out of various types of ground, terrain, and obstacles. The basic tenets of mobile propagation are, e.g., reflection, diffraction, and scattering.

A mobile receiver is often surrounded by various obstacles. The incoming waves arrive from different angles with different propagation delays. The signal is in the form of reflections, diffractions, and scattering caused by several obstacles [1]. This is known as *multipath propagation*. Figure 1.1 presents typical signal propagation paths from base station to mobile station. Furthermore, the signal components arriving along different paths at the receiver undergo different frequencies due to the motion between transmitter and receiver, which depends on velocity and direction of motions of the mobiles. This also has an influence on the transmission characteristics of the mobile radio channel and leads to *Doppler effect*.

The signal received by the mobile may consist of a number of plane waves having randomly distributed amplitudes, phases, and angles of arrival. The sum of the multiple waves at the receiver results in a signal that fluctuates rapidly as the receiver and/or the transmitter moves. This signal fluctuation is known as *fading*, which is caused by interference between two or more versions of the transmitted signal arrived at the receiver at different times.

The signal strength can be separated into two parts called long-term fading and short-term fading. The long-term signal fading is referred to the path loss or signal power attenuation due to the motion over large areas. It is mainly caused by terrain configuration and the built or man-made obstacles between the base station and the mobile unit. The receiver is often represented as shadowing in this case. Terrain configurations can be classified as open area, flat terrain, hilly terrain, and mountain area. The man-made landscape can be classified as rural area, suburban terrain, and urban terrain.

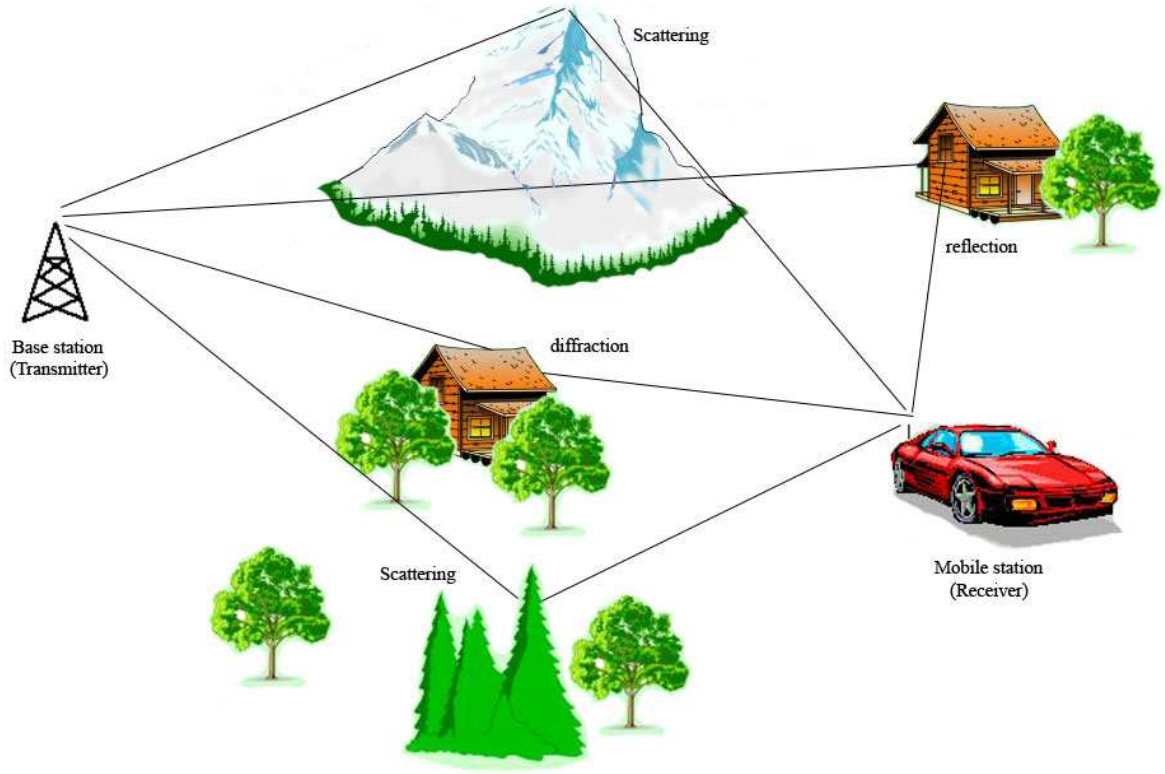

Figure 1.1: Multipath propagation

The short-term fading is mainly caused by multipath reflections of a transmitted wave by local scatterers, such as buildings or natural obstacles. It indicates changes in the signal that can be experienced as a result of small changes between the transmitter and the receiver. The short-term fading manifests itself in time-spreading of the signal (signal dispersion) and time-variant of the channel. The channel for mobile radio applications is time-variant, because motion between transmitter and receiver results in propagation path changes.

1.3 Problem Description

Mobile channels are naturally random and results, therefore, in uncontrolled reflection, scattering, shadowing and attenuation of the transmitted signal. It may be impracticable to detect the transmit signal correctly due to the superposition of different signal waves at the receiver. These effects can be statistically modeled as a multiple random variable and are referred to as fading, which is one of the main problems in mobile communication. This variation can also be an advantage in a multiuser system, as different users undergo different time-varying receiving conditions. Furthermore, there are many propagation paths

between a transmitter and a receiver in mobile communication with various delays at the receiver. The knowledge of multipath fading channel characteristics is essential to get on with problems faced during the development of mobile communication systems. To characterize such channel behavior, different channel models have been developed, such as the elliptical [6, 18, 32] or the ring model [10]. In this thesis, I follow an other approach to model statistical properties of the channel. Here, specifications of a street, e.g., the size of buildings or the motion of the transmitter and the receiver with respect to the obstacles, determine the basic of the geometrical street model. Furthermore, improvements of communication systems, such as the high link quality or higher data rates, are needed. This can be obtained by the use of the multiple-input multiple-output (MIMO) systems. Therefore, this thesis is devoted to the problem of modeling, analyzing, and simulating the mobile-to-mobile MIMO street model.

Mobile-To-Mobile Communication

Mobile-to-mobile communication is referred to as the transmitter and the receiver are both in motion. This is expected to play an important role in mobile ad hoc networks and intelligent transportation systems, where the communication links should be extremely reliable. An increasing number of communication standards, such as Bluetooth, require mobile terminals to communicate directly with other mobile terminals instead of a base station. The received signal strength is caused to fluctuate and the signal will nearly change as the movement occurs, since the multipath fading in an environment is known. In the literature, the mobile-to-mobile communication models have been investigated in [2, 3, 19, 30, 31], whereas the geometrical two-ring scattering model for MIMO mobile-to-mobile fading channels are introduced in [2, 3, 31].

Channel Model

For the design and analysis of mobile communication systems, channel modeling plays an important part. In general, the channel models for mobile radio communication are based on the use of at least two colored Gaussian noise processes [1]. For instance, two real colored Gaussian noise processes are required for the realization of a Rayleigh or Rice process, which are often used as related stochastical models for describing the fading behavior of the envelope of the received signal through mobile radio channels. Furthermore, a general approach to describe the channel is to assume that the transmitted radio waves act as plane waves from different directions due to the multipath propagation. A statistical description of such mobile radio channels has been developed by Clarke [23] and Jakes [24]. A channel modeling strategy is the statistical description of time variant fading effects due to the motion of mobiles, obstacles and the transmission environment.

Random Variables

Random variables are important for the modeling of mobile fading channels and the channel

is modeled with stochastic components. Therefore, the channel parameters are considered as outcomes of a random process and are random variables. In this work, random variables are described by their probability density function (PDF), followed by their power spectral density function (PSD), and their autocorrelation function (ACF).

1.4 Thesis Overview

In this thesis, the geometrical street model for mobile-to-mobile channel is considered under the assumption that the transmitter and the receiver are moving. The proposed procedure is a generalization of the principle of deterministic channel modeling, i.e.,

1. Computation of a geometrical model, whereas the street model is analyzed
2. Derivation of a stochastic analytical model from the geometrical model
3. Determination of the deterministic simulation model by fixing model parameters of the stochastic simulation model
4. Computation of the model parameters from the simulation model by using a proper parameter computation method, e.g., L_p-norm method
5. Generation of sample functions by using the deterministic simulation model with fixed parameters.

This principle is closely related to the sum-of-sinusoids method, which was originally proposed by Rice to model Gaussian noise processes [12]. The illustration of the generalized principle of deterministic channel modeling is shown in Fig. 1.2.

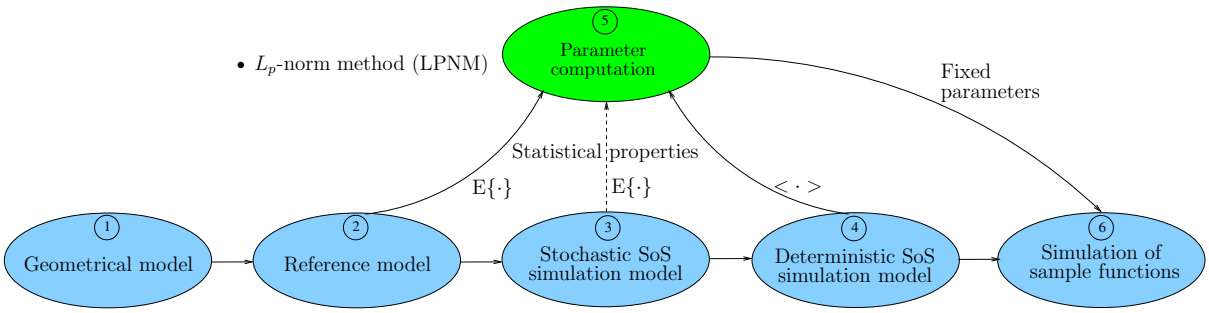

Figure 1.2: The principle of deterministic channel modelling

Chapter 2 gives a description of the geometrical street model for a wireless transmission between the transmitter and the receiver. The relation between the transmitting and

receiving angles are also established as a function of the parameters describing the geometrical street model.
Chapter 3 presents the derivation of an analytical model over the geometrical model and also results concerning the statistical properties of such channel model due to scattering from a cluster.
The simulation model derived from the analytical model is presented in Chapter 4, as well as the parameter computation method L_p-norm, and simulation results in comparison to the analytical model. Chapter 5 shows the extension of the simple SISO street model with respect to multiple clusters of scatterers, frequency selectivity, and MIMO street model.
The discussion of the thesis is given in Chapter 6 and the conclusion of the thesis is presented in Chapter 7. The list of literature completes this thesis.

Chapter 2

Geometrical Model

Geometrical channel models have been submitted in the literature for different propagation environments due to the fact that the geometrical approach provides analytically solutions. For instance, Liberti and Rappaport developed a geometrical based single bounce model (GBSBM) for microcells which assumes that the scatterers lie in an ellipse encompassing the transmitter and receiver [6]. In addition, a disk model is investigated in [7, 8] which based on the Jakes model and a ring model has been proposed in [9, 10] for the MIMO channel.
This chapter describes the geometrical model for a transmission between two mobiles so-called SISO mobile-to-mobile channel, i.e., there is a single antenna at both ends of the channel, whereas the transmitter and the receiver are on the move. Moreover, the relation between angle of departure (AOD) and angle of arrival (AOA) are presented, which will be used for the derivation of the statistical properties of the geometrical street model described in the next chapter.

2.1 The Street Model

In this section, the geometrical street model for the mobile-to-mobile SISO channel is described as shown in Fig. 2.1. It is assumed that there is a single reflected wave on the surface of the scattering object between the transmitter and the receiver. This figure shows that all scatterers associated with a certain path length l can be emerged to a cluster, which form the geometrical street model. The scatterers along the street are fixed and can be, for example, trees, buildings, hills, etc. Buildings are normally structured not perfectly smooth as reflecting objects. Therefore, they are mostly considered as a cluster of scatterers instead of a reflector. The scatterers in a cluster are assumed to be uniformly distributed.

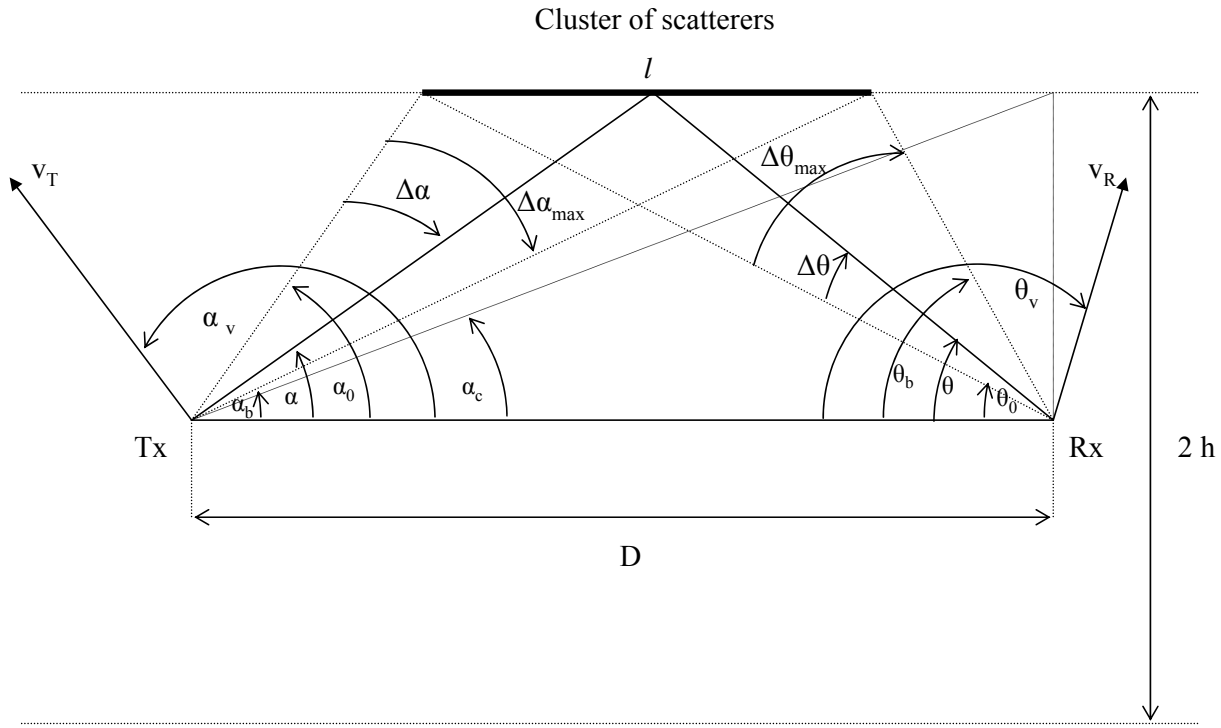

Figure 2.1: The geometrical street model with a single cluster of scatterers

As you can see in Fig. 2.1, the transmitter T_x and the receiver R_x are separated by a distance D and located in the middle between the roadsides with the street width $2h$. The angle of departure (AOD) and the angle of arrival (AOA) can be characterized by α and θ, respectively. The angles of departure α are between α_0 and α_c, where α_c represents the critical angle of departure due to the structure of the street model. Therefore, the restricted angle of arrival θ must be between θ_0 and θ_c. Thus, $\alpha = \alpha_0 - \Delta\alpha$ ($\theta = \theta_0 - \Delta\theta$), where $\Delta\alpha$ ($\Delta\theta$) represents the angle of spreading and is a random variable. It is also assumed that the transmitter and the receiver are on the move as shown in Fig. 2.1. The direction of motion at the transmitter (receiver) is characterized by α_v (θ_v), where v_T (v_R) is referred to as the speed of the transmitter (receiver).

2.2 Relation Between AOD and AOA

The relationship between the AOD α and the AOA θ is given by using the properties of the geometry. For the determination of statistics of the received signal, it is important to know characteristic quantities, such as the probability density function of the angle of arrival (PDF of AOA), the Doppler power spectral density function (PSD), the autocorrelation function (ACF), the level-crossing rate (LCR), and the average duration of fades (ADF).

The AOD α and the AOA θ depend on the environment surrounding the transmitter and the receiver. For instance, the mobiles are often surrounded by obstacles and there maybe no line of sight. Such models are investigated, e.g., in [2, 10]. For the geometrical street model, the AOA θ can be expressed in terms of the AOD α as

$$\theta = f_\theta(\alpha) = \begin{cases} f(\alpha) & \alpha_b \leq |\alpha| < \alpha_0 \\ \pm\frac{\pi}{2} & \alpha = \pm\alpha_c \\ \pm\alpha_c & \alpha = \pm\frac{\pi}{2} \\ 0 & else \end{cases} \tag{2.1}$$

where

$$f(\alpha) = \arctan\left(\frac{h\tan(\alpha)}{D\tan(\alpha) - h}\right) \tag{2.2}$$

and

$$\begin{aligned} \alpha_c &= \arctan\left(\frac{h}{D}\right) \\ \alpha_c &\leq \alpha_b < \alpha_0 \\ \alpha_b &< \alpha_0 \leq \frac{\pi}{2}. \end{aligned} \tag{2.3}$$

The quantity α_c is referred to as the critical AOD, because the receiver cannot receive scattered components, when the AOA θ is larger than $\pi/2$, as one can see in Fig. 2.1. Furthermore, the AOD α is in the interval $[\alpha_0, \alpha_b]$ for the street model. It is also considered that $f_\theta(\alpha)$ is a bijective function. Therefore, the AOD α can be derived as a reverse function of θ and denoted by

$$\alpha = \begin{cases} g(\theta) & \theta_0 \leq |\theta| < \theta_b \\ \pm\frac{\pi}{2} & \theta = \pm\theta_c \\ \pm\theta_c & \theta = \pm\frac{\pi}{2} \\ 0 & else \end{cases} \tag{2.4}$$

where

$$g(\theta) = \arctan\left(\frac{h\tan(\theta)}{D\tan(\theta) - h}\right) \tag{2.5}$$

and

$$\begin{aligned} \theta_c &= \alpha_c \\ \theta_c &< \theta_0 < \theta_b \\ \theta_0 &< \theta_b \leq \frac{\pi}{2}. \end{aligned} \tag{2.6}$$

Since the relation between the AOD α and AOA θ is found, the statistical properties of the street channel model can thereby be derived and described in the next chapter.

Chapter 3

Stochastic Analytical Model

After providing the geometrical street model, the next step of deterministic channel modeling is to derive a stochastic analytical model from the geometrical model. The main purpose of this step is to find stochastic processes that are suitable for frequency non-selective models. The analytical or reference model is described by ideal stochastic processes. The derivation of the analytical model is firstly performed under the assumption that the numbers of scatterers are infinite. Then, the statistical properties of the reference model are analyzed in terms of the probability density function of the angle of arrival (PDF of AOA), the Doppler power spectral density (PSD), the temporal autocorrelation function (ACF), the level-crossing rate (LCR), and the average duration of fades (ADF).

3.1 Probability Density Function

The PDF of AOA of a scattered wave is important for the derivation of the statistical properties of the channel, such as the power spectral density and the signal correlation function at the receiver. In [4, 5] a geometrically based PDF of AOA is derived by using cosine PDF for non-isotropic scattering models. Such a model is obtained, when signals are channeled, e.g., along a city street. In this appraoch, the derivation of the PDF of the AOA at the receiver, I will follow the geometrical street model presented in Fig. 2.1.

Since $\alpha = \alpha_0 - \Delta\alpha$ and $\theta = \theta_0 + \Delta\theta$, the function of $\Delta\theta$ can be determined as an expression of $\Delta\alpha$ by using (2.1) as

$$\Delta\theta = f(\alpha_0 - \Delta\alpha) - \theta_0, \tag{3.1}$$

where

$$f(\alpha_0 - \Delta\alpha) = \arctan\left(\frac{h\tan(\alpha_0 - \Delta\alpha)}{D\tan(\alpha_0 - \Delta\alpha) - h}\right). \tag{3.2}$$

The function (3.1) holds, if $0 \leq \Delta\alpha \leq \alpha_0 - \alpha_b$, where α_0 and α_b are given by (2.3). Thus, the function of $\Delta\alpha$ can be expressed in terms of $\Delta\theta$ by using (2.4) as

$$\Delta\alpha = \alpha_0 - g(\theta_0 + \Delta\theta), \tag{3.3}$$

where

$$g(\theta_0 + \Delta\theta) = \arctan\left(\frac{h\tan(\theta_0 + \Delta\theta)}{D\tan(\theta_0 + \Delta\theta) - h}\right), \tag{3.4}$$

if $0 \leq \Delta\theta \leq \theta_b - \theta_0$, where θ_b and θ_0 are define by (2.6). In Addition, θ_0 is determined by (2.1) at $\alpha = \alpha_0$, i.e.,

$$\theta_0 = f_\theta(\alpha_0) = \begin{cases} f(\alpha_0) & \alpha_b < |\alpha_0| < \frac{\pi}{2} \\ \pm\frac{\pi}{2} & \alpha_0 = \pm\alpha_c \\ \pm\alpha_c & \alpha_0 = \pm\frac{\pi}{2} \\ 0 & else. \end{cases} \tag{3.5}$$

Under the assumption that $\Delta\alpha$ is a uniformly distributed random variables, the PDF of the angle of spreading $p_{\Delta\alpha}(\Delta\alpha)$ is assumed to be

$$p_{\Delta\alpha}(\Delta\alpha) = \frac{1}{\Delta\alpha_{\max}}, \tag{3.6}$$

where $\Delta\alpha_{\max}$ indicates the maximum angle of spreading at the transmitter in the interval $[0, \alpha_0 - \alpha_b]$, since the cluster of scatterers is confined between the transmitter and the receiver. The PDF of $\Delta\theta$ can be derived from the given PDF of $\Delta\alpha$ by using following random variable transformation

$$\begin{aligned} p_{\Delta\theta}(\Delta\theta) &= \frac{p_{\Delta\alpha}(\Delta\alpha)}{\left|\frac{d_{\Delta\theta}(\alpha)}{d\Delta\alpha}\right|} \\ &= \frac{p_{\Delta\alpha}(\Delta\alpha)}{\left|\frac{d(f_\theta(\alpha_0 - \Delta\alpha) - \theta_0)}{d\Delta\alpha}\right|} \\ &= \frac{p_{\Delta\alpha}(\Delta\alpha)}{\left|\frac{d(f_\theta(\alpha_0 - \Delta\alpha))}{d\Delta\alpha}\right|} \end{aligned} \tag{3.7}$$

where

$$\left|\frac{df_\theta(\alpha_0 - \Delta\alpha)}{d\Delta\alpha}\right| = \left|\frac{h^2}{h^2 + D^2\sin^2(\Delta\alpha - \alpha_0) + 2Dh\sin(\Delta\alpha - \alpha_0)\cos(\Delta\alpha - \alpha_0)}\right|.$$

Substitute (3.6) in (3.7) and using (3.3) together with (2.5) as a definition of $\Delta\alpha$, the PDF of the angular spread $p_{\Delta\theta}(\Delta\theta)$ can be plotted as shown in Fig. 3.1.

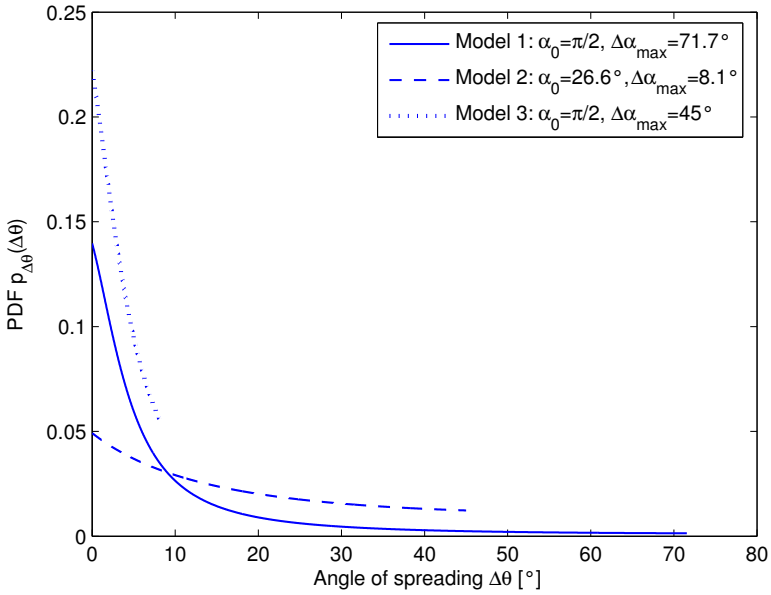

Figure 3.1: The PDF of the angle of spreading $\Delta\theta$ for various values of α_0 and $\Delta\alpha_{\max}$

The three Models for various values of the length l and the position of a cluster are considered with $D = 15$ and $h = 5$:

- Model 1: $l = 15$, $\alpha_0 = \frac{\pi}{2}$, $\alpha_b = 18.4^o$, $\Delta\alpha_{\max} = 71.7^o$,
  the corresponding angles $\theta_0 = 18.4^o$ and $\Delta\theta_{\max} = 71.7^o$
- Model 2: $l = 5$, $\alpha_0 = 26.6^o$, $\alpha_b = 18.4^o$, $\Delta\alpha_{\max} = 8.1^o$,
  the corresponding angles $\theta_0 = 45^o$ and $\Delta\theta_{\max} = 45^o$
- Model 3: $l = 5$, $\alpha_0 = \frac{\pi}{2}$, $\alpha_b = 45^o$, $\Delta\alpha_{\max} = 45^o$,
  the corresponding angles $\theta_0 = 18.4^o$ and $\Delta\theta_{\max} = 8.1^o$

It should be noted that the length and the position of a cluster are defined by α_0 and α_b. As one can see in the geometrical street model Fig. 2.1, the length of a cluster can be also given by $\Delta\alpha_{\max}$. Figure 3.1 shows the influence of different positions and lengths of a cluster on the PDF $p_{\Delta\theta}(\Delta\theta)$ of the angle of spreading.

Next, the relationship of the street width h and the distance between the transmitter and the receiver D for $l = 15$ are considered as follows:

- Model 1: $\frac{h}{D} = 0.1$, the corresponding angles $\theta_0 = 5.7^o$, $\Delta\theta_{\max} = 84.3^o$
- Model 2: $\frac{h}{D} = 0.3$, the corresponding angles $\theta_0 = 18.4^o$, $\Delta\theta_{\max} = 71.6^o$
- Model 3: $\frac{h}{D} = 0.5$, the corresponding angles $\theta_0 = 26.6^o$, $\Delta\theta_{\max} = 63.4^o$

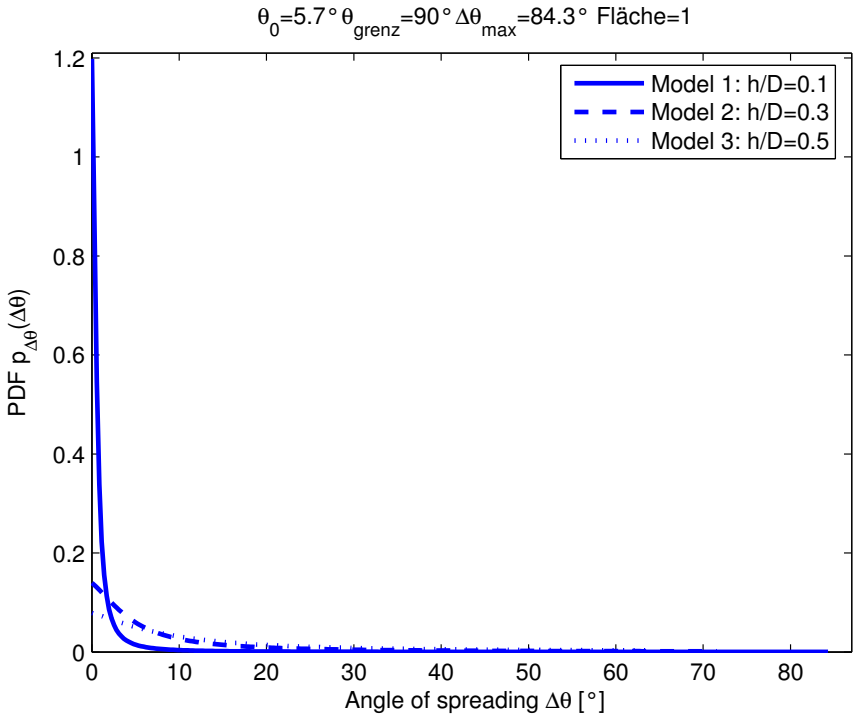

Figure 3.2: The PDF of the angle of spreading $\Delta\theta$ for various values of h/D ($l = 15$)

The influence of the relation between h and D on the PDF of the angle of spreading at the receiver $p_{\Delta\theta}(\Delta\theta)$ is shown in Fig. 3.2 with $\alpha_0 = \pi/2$.

In order to describe the statistical properties of the street model with a single cluster of scatterers, the temporal autocorrelation function (ACF) is of importance. Therefore, the Doppler power density function (PSD) plays an importance role, since the ACF of the scattered component is defined as the inverse Fourier transform of the Doppler PSD.

3.2 Doppler Power Spectral Density

Due to the motion of the transmitter and the receiver (mobile-to-mobile), the Doppler effect arises, which also depends on the direction of motions of the transmitter and the receiver. When the transmitter and receiver move with time, fading will impose a varying envelope on a transmitted signal, thus spreading the spectrum of the received signal [14]. This is known as *Doppler spreading*. In a multipath channel, each transmitted signal with the AOD $\alpha = \alpha_0 - \Delta\alpha$ undergoes a different Doppler frequency shift during its transmission. The Doppler frequency (frequency shift) at the receiver under the AOA $\theta = \theta_0 + \Delta\theta$ is

given by

$$f = s(\Delta\alpha, \Delta\theta) = f_{T_{\max}} \cos(\alpha_v - \alpha_0 + \Delta\alpha) + f_{R_{\max}} \cos(\theta_v - \theta_0 - \Delta\theta) \tag{3.8}$$

where $f_{T_{\max}}$ and $f_{R_{\max}}$ stand for the maximum Doppler frequency of the transmitter and the receiver, respectively. The α_v (θ_v) is the angle of the direction of the transmitter (receiver) from the line of sight as shown in Fig. 2.1. The maximum Doppler frequency of the transmitter $f_{T_{\max}}$(receiver $f_{R_{\max}}$) is related to the speed of the transmitter v_T (receiver v_R), the speed of light in vacuum c_0, and the carrier frequency f_0. The maximum Doppler frequencies can be expressed as

$$f_{T_{\max}} = \frac{v_T}{c_0} f_0 \qquad ; \qquad f_{R_{\max}} = \frac{v_R}{c_0} f_0. \tag{3.9}$$

The equation (3.8) shows that the Doppler frequency f is a function of the quantities $\Delta\alpha$ and $\Delta\theta$, which are referred to as random variables in the street model. By the use of a relation between $\Delta\alpha$ and $\Delta\theta$, the corresponding densities can also be derived as shown in (3.6) and (3.7). Since the PDF of $\Delta\alpha$ and $\Delta\theta$ are given, the PDF of the Doppler frequency $p_f(f)$ can be computed by using the random variable transformation described in [13]. Here, the quantities $\Delta\alpha$ and $\Delta\theta$ are stochastically dependent on each other that is $\Delta\theta = f(\Delta\alpha)$. Therefore, the derivation of $p_f(f)$ becomes more complicated with the substitutions of (3.3) and (3.4) in (3.8). Moreover, a closed form solution for the inverse function $\Delta\theta = s^{-1}(f)$ could not be derived, but it is necessary since the number of solutions for $\Delta\theta = s^{-1}(f)$ is needed to determine $p_f(f)$ by the random variable transformation [13]. Hence, the Doppler PSD of the mobile-to-mobile street model will be derived by an alternative method with the definition of the autocorrelation function (ACF) described in the next section, since the Doppler PSD and the ACF are a Fourier transform pair.

For simplicity, it is assumed that the transmitter is fixed (v_T=0) and the receiver moves with the direction of motion θ_v and the speed v_R, the Doppler frequency (3.8) can be therefore expressed as

$$f = f_{R_{\max}} \cos(\theta_v - \theta_0 - \Delta\theta), \tag{3.10}$$

where θ_v is in the interval $(0, 2\pi]$. It should be noted that two solutions exist, i.e., $\arccos(f/f_{R_{\max}}) = (\theta_v - \theta) = (\theta - \theta_v)$ due to the inverse function of the cosine function. The PDF of the Doppler frequency $p_f(f)$ can be derived from the PDF of the angle spreading $p_{\Delta\theta}(\Delta\theta)$ by the use of the transformation of a random variable in the form

$$p_f(f) = \frac{p_{\Delta\theta}(\theta_v - \theta_0 - \left|\arccos\frac{f}{f_{R_{\max}}}\right|)}{f_{R_{\max}}\sqrt{1 - \left(\frac{f}{f_{R_{\max}}}\right)^2}} + \frac{p_{\Delta\theta}(\theta_v - \theta_0 + \left|\arccos\frac{f}{f_{R_{\max}}}\right|)}{f_{R_{\max}}\sqrt{1 - \left(\frac{f}{f_{R_{\max}}}\right)^2}} \tag{3.11}$$

for $|f| \leq f_{R_{\max}}$. Since the PDF $p_f(f)$ is proportional to the Doppler PSD [1], it follows the

relation

$$S_{\mu\mu}(f) = 2\sigma_0^2 p_f(f) \tag{3.12}$$
$$= \frac{2\sigma_0^2}{f_{R_{\max}}\sqrt{1-\left(\frac{f}{f_{R_{\max}}}\right)^2}}\left[p_{\Delta\theta}\left(\theta_v-\theta_0-\left|\arccos\frac{f}{f_{R_{\max}}}\right|\right)+p_{\Delta\theta}\left(\theta_v-\theta_0+\left|\arccos\frac{f}{f_{R_{\max}}}\right|\right)\right]$$

where $2\sigma_0^2$ is the mean power of the received scattered components. The Doppler PSD is bounded within the range of lower and upper frequency $[f_l, f_u]$, whereas f_l and f_u are given by

$$f_u = \begin{cases} f_{R_{\max}}\cos(\theta_0-\theta_v) & 0<\theta_v<\theta_0 \\ f_{R_{\max}} & \theta_0<\theta_v<\theta_b \\ f_{R_{\max}}\cos(\theta_v-\theta_b) & else \end{cases} \tag{3.13}$$

and

$$f_l = \begin{cases} f_{R_{\max}}\cos(\theta_b-\theta_v) & 0<\theta_v<\frac{\theta_0+\theta_b}{2} \\ -f_{R_{\max}} & \theta_0<\theta_v-\pi<\theta_b \\ f_{R_{\max}}\cos(\theta_v-\theta_0) & else \end{cases} \tag{3.14}$$

where θ_b determines the maximum possible AOA and the direction of motion at the receiver θ_v is in the range of $(0, 2\pi]$. The Doppler PSD is exemplarily plotted in Fig. 3.3.

In this case, the receiver is moving with the speed $v_R = 50$km/h and in the direction $\theta_v = 120^o$. Furthermore, the Doppler frequency is normalized by $f_{R_{\max}}$. Figure 3.3 shows the corresponding Doppler PSD of three models for various values of the length l and the position of a cluster with $D = 15$, $h = 5$, and $\sigma_0 = 0.5$:

- Model 1: $l = 15$, $\Delta\theta_{\max} = 71.7^o$
  the frequency range is from $f_l = -8.4$ Hz to $f_u = 36.1$ Hz
- Model 2: $l = 5$, $\Delta\theta_{\max} = 45^o$
  the frequency range is from $f_l = 10.8$ Hz to $f_u = 36.1$ Hz
- Model 3: $l = 5$, $\Delta\theta_{\max} = 8.1^o$
  the frequency range is from $f_l = -8.4$ Hz to $f_u = -2.5$ Hz

Moreover, the influence of the relation between h and D on the PSD is shown in Fig. 3.4 with the same given values as in Fig. 3.2.

The Doppler PSD gives the average power of the scattering components and is proportional to the probability density function of the Doppler frequencies $p_f(f)$. There are two

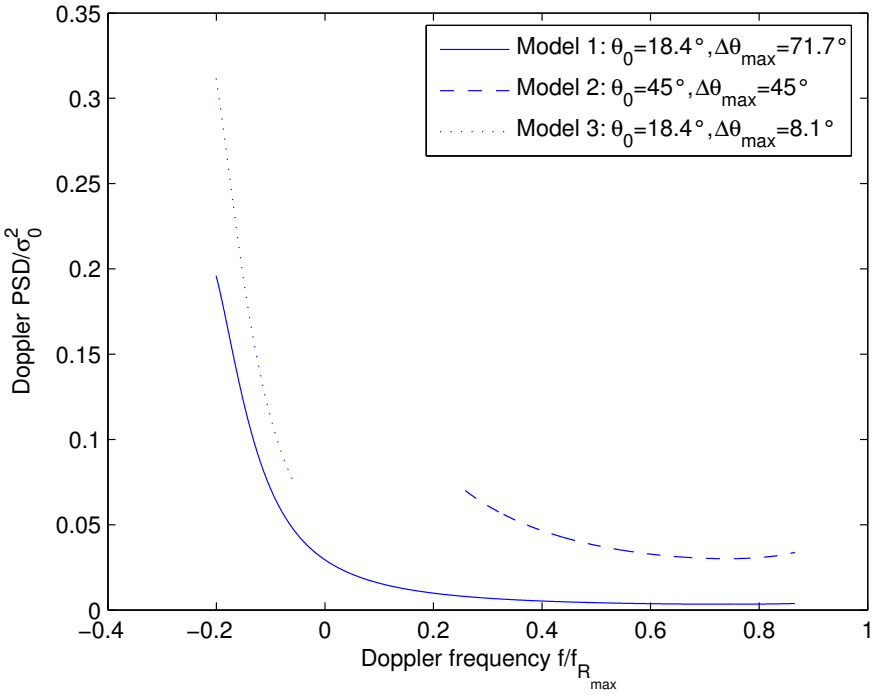

Figure 3.3: The Doppler PSD for various values of $\Delta\theta_{\max}$ ($D = 15, h = 5, f_{R_{\max}} = 41.7$ Hz, $\sigma_0 = 0.5$)

characteristic quantities, which can be derived from the Doppler PSD. These quantities are the average Doppler shift $B_{\mu\mu}^{(1)}$ and the Doppler spread $B_{\mu\mu}^{(2)}$, which describes the average frequency shift and the frequency spread, respectively. The Doppler shift $B_{\mu\mu}^{(1)}$ is expressed as

$$\begin{aligned} B_{\mu\mu}^{(1)} &= \frac{\int_{-\infty}^{\infty} f S_{\mu\mu}(f) df}{\int_{-\infty}^{\infty} S_{\mu\mu}(f) df} \\ &= \frac{1}{2\pi j} \cdot \frac{\dot{r}_{\mu\mu}(0)}{r_{\mu\mu}(0)} \end{aligned} \tag{3.15}$$

and the Doppler spread $B_{\mu\mu}^{(2)}$ is defined by

$$\begin{aligned} B_{\mu\mu}^{(2)} &= \sqrt{\frac{\int_{-\infty}^{\infty} (f - B_{\mu\mu}^{(1)})^2 S_{\mu\mu}(f) df}{\int_{-\infty}^{\infty} S_{\mu\mu}(f) df}} \\ &= \frac{1}{2\pi} \sqrt{\left(\frac{\dot{r}_{\mu\mu}(0)}{r_{\mu\mu}(0)}\right)^2 - \frac{\ddot{r}_{\mu\mu}(0)}{r_{\mu\mu}(0)}}. \end{aligned} \tag{3.16}$$

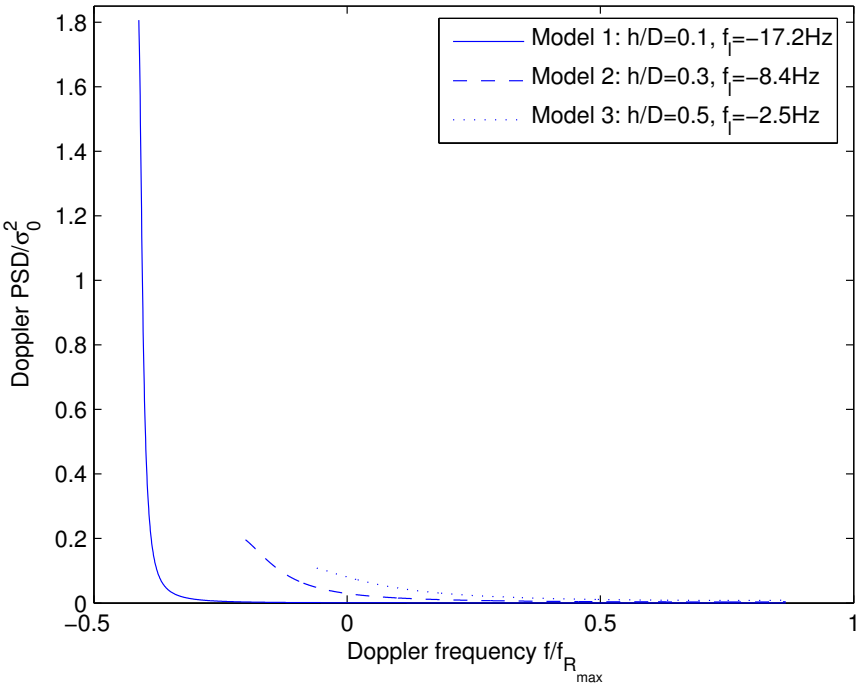

Figure 3.4: The Doppler PSD for various values of h/D ($f_u = 36.1$ Hz, $f_{R_{\max}} = 41.7$ Hz, $\sigma_0 = 0.5$)

3.3 Autocorrelation Function

The Autocorrelation function (ACF) is one of the functions that can be extracted from the first order statistics of the received signal. In general, if the received signal is in the complex baseband described by a zero-mean complex Gaussian random process $\mu(t) = \mu_1(t) + j\mu_2(t)$, the ACF can be defined by [13]

$$\begin{aligned} r_{\mu\mu}(\tau) &= E\{\mu^*(t)\mu(t+\tau)\} \\ &= r_{\mu_1\mu_1}(\tau) + r_{\mu_2\mu_2}(\tau) + j\left[r_{\mu_1\mu_2}(\tau) - r_{\mu_2\mu_1}(\tau)\right] \end{aligned} \tag{3.17}$$

where $E\{\cdot\}$ denotes the statistical expected value. Generally, it is assumed that $\mu_1(t)$ and $\mu_2(t)$ represent real-valued Gaussian processes and are uncorrelated [1]. The principle of the sum-of-sinusoids, which will be also introduced in Chapter 4, is based on the superposition of an infinite number of weighted harmonic functions. Due to this principle, a Gaussian process $\mu(t)$ can be expressed mathematically as

$$\mu(t) = \lim_{N\to\infty} \sum_{n=1}^{N} c_n e^{j(2\pi f_n t + \theta_n)}, \tag{3.18}$$

where c_n, f_n, and N denote the Doppler coefficients, the Doppler frequencies, and the number of harmonic functions, respectively. The phases θ_n are random variables with a

uniform distribution in the interval $(0, 2\pi]$. Since the number of exponential functions N is infinite, a channel model is described by non-realizable stochastic processes as the reference model or the analytical model. Then, the ACF can be specified as

$$r_{\mu\mu}(\tau) = \lim_{N\to\infty} \sum_{n=1}^{N} c_n^2 e^{j(2\pi f_n \tau)}. \tag{3.19}$$

Moreover, it is also mentioned that the ACF $r_{\mu\mu}(\tau)$ is the inverse Fourier transformation of the Doppler spectral density function $S_{\mu\mu}(\tau)$ and given by

$$r_{\mu\mu}(\tau) = \mathcal{F}^{-1}\left\{S_{\mu\mu}(f)\right\} = \int_0^f S_{\mu\mu}(f) e^{j2\pi f\tau} df, \tag{3.20}$$

where $\mathcal{F}^{-}1\{\cdot\}$ denotes the inverse Fourier transform. For the case that the transmitter is fixed and the receiver moves, the ACF $r_{\mu\mu}(\tau)$ has been determined by using the inverse Fourier transform of (3.12). The absolute value of the ACF $r_{\mu\mu}(\tau)$ is plotted in Fig. 3.5, which shows the influence of different positions and lengths l of a cluster. The parameters $l, \Delta\theta_{\max}, f_{R_{\max}}, D, h$, and σ_0 are specified the same as those in Fig. 3.3. As it is shown in

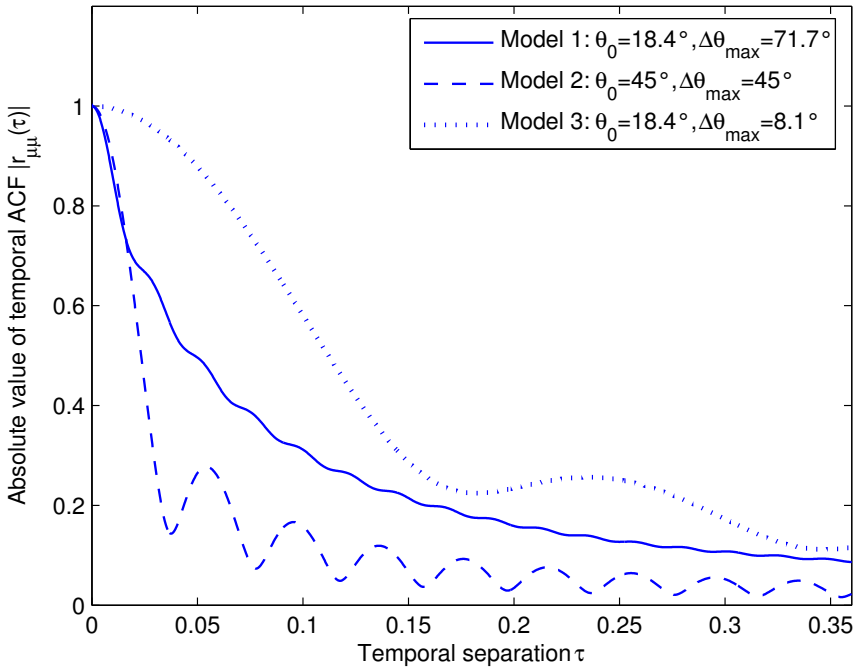

Figure 3.5: The absolute value of ACF for various values of $\Delta\theta_{\max}$ ($D = 15, h = 5, f_{R_{\max}} = 41.7$ Hz, $\sigma_0 = 0.5$)

Fig. 3.5, the third model with the quantities $l = 5$, $\alpha_0 = \pi/2$, and $\Delta\alpha_{\max} = 45^o$ is kept constant at the beginning compared to the other two models. The second model with the same length of a cluster but a different initial angle of departure α_0 is greatly decreased.

Once again, the relation between h and D is considered with the same specified values as in Fig. 3.4 and plotted in Fig. 3.6. As a result, the correlation of the received signal of the first model increases greatly, compared to the other two models.

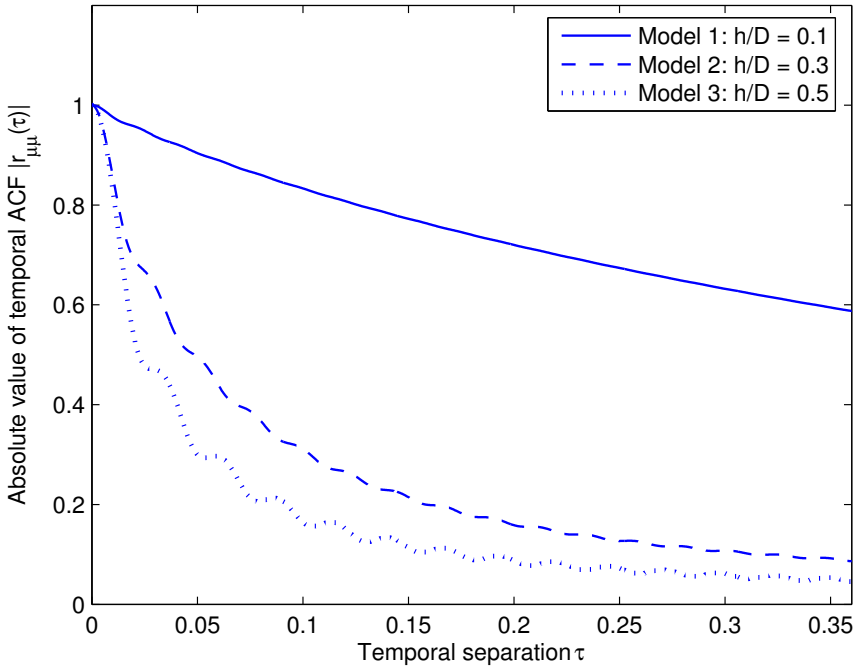

Figure 3.6: The absolute value of ACF for various values of h/D ($f_{R\max} = 41.7$ Hz, $\sigma_0 = 0.5$)

Now, the mobile-to-mobile communication system is taken into consideration, i.e., the transmitter and the receiver are on the movements with angles of motion α_v and θ_v as shown in Fig. 2.1. The ACF is given by

$$r_{\mu\mu}(\tau) = \rho_T(\tau) \cdot \rho_R(\tau), \tag{3.21}$$

where $\rho_T(\tau)$ and $\rho_R(\tau)$ can be expressed as

$$\rho_T(\tau) = \int_0^{\Delta\alpha_{\max}} e^{-j2\pi f_T(\Delta\alpha)\tau} p_{\Delta\alpha}(\Delta\alpha) d\Delta\alpha \tag{3.22}$$

$$\rho_R(\tau) = \int_0^{\Delta\theta_{\max}} e^{-j2\pi f_R(\Delta\theta)\tau} p_{\Delta\theta}(\Delta\theta) d\Delta\theta. \tag{3.23}$$

The $f_T(\Delta\alpha)$ and $f_R(\Delta\theta)$ are referred to the Doppler frequency at the transmitter and the receiver, respectively, and are defined by the direction of arrival of each wave and the

direction of motions according to the relation

$$f_T(\Delta\alpha) = f_{T_{\max}} \cos(\alpha_v - \alpha_0 + \Delta\alpha) \tag{3.24}$$

$$f_R(\Delta\theta) = f_{R_{\max}} \cos(\theta_v - \theta_0 - \Delta\theta). \tag{3.25}$$

Since angles of motions of the transmitter and the receiver have an effect on the ACF, the three cases concerning different directions of the motions of the mobiles are investigated and plotted in Fig. 3.7:

- Model 1: $\alpha_v = 50^o$, $\theta_v = 50^o$
  (the transmitter and the receiver move to each other)
- Model 2: $\alpha_v = 50^o$, $\theta_v = 120^o$
  (the transmitter and the receiver move in one direction)
- Model 3: $\alpha_v = 120^o$, $\theta_v = 120^o$
  (the transmitter and the receiver move apart)

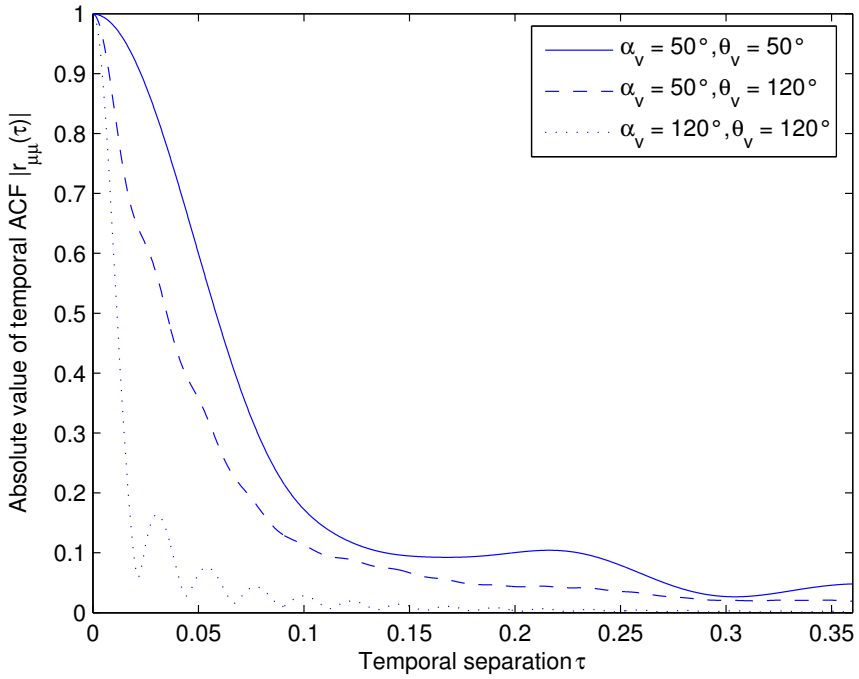

Figure 3.7: The absolute value of ACF for mobile-to-mobile channel with different direction of motions of the transmitter and the receiver ($D = 15, h = 5, f_{T\max} = 41.7$ Hz, $f_{R\max} = 41.7$ Hz, $\sigma_0 = 0.5$)

It is shown in Fig. 3.7 that the ACF is decreased rapidly, when the transmitter and the receiver are moving apart from each other.

Furthermore, the ACF $r_{\mu\mu}(\tau)$ is a complex value due to the asymmetrical shape of the resulting PSD $S_{\mu\mu}(f)$. In the next section, the definition of two factors resulting from the ACF of the complex Gaussian random process $\mu(t)$ will be applied for the derivation of the level-crossing rate and the average duration of fades. These factors can be defined from the ACF given in (3.17) as

$$\psi_0^{(n)} = \frac{d^n}{d\tau^n} r_{\mu_1\mu_1}(\tau)|_{\tau=0} \tag{3.26}$$

$$\phi_0^{(n)} = \frac{d^n}{d\tau^n} r_{\mu_1\mu_2}(\tau)|_{\tau=0}. \tag{3.27}$$

Thus, they can be expressed for $n = 0, 1, 2$ as

$$\ddot{\psi}_0 = \psi_0^{(2)} = \frac{d^2}{d\tau^2} r_{\mu_1\mu_1}(0) \tag{3.28}$$

$$\dot{\phi}_0 = \phi_0^{(1)} = \frac{d}{d\tau} r_{\mu_1\mu_2}(0) \tag{3.29}$$

$$\psi_0 = r_{\mu_1\mu_1}(0). \tag{3.30}$$

As $r_{\mu_1\mu_1} = r_{\mu_2\mu_2}$ and $r_{\mu_1\mu_2} = -r_{\mu_2\mu_1}$ [1], one can introduce $Re\{r_{\mu\mu}\} \cdot 1/2 = r_{\mu_1\mu_1}$ and $Im\{r_{\mu\mu}\} \cdot 1/2 = r_{\mu_1\mu_2}$, which has been used together with (3.17) for the analytical derivation of $\ddot{\psi}_0, \phi_0$, and ψ_0.

3.4 Level-Crossing Rate

Beside the PDF of AOA, the PSD, and the ACF, the level-crossing rate (LCR) and the average duration of fades (ADF) are also the characteristic quantities describing the statistics of mobile radio channels. The LCR and the ADF are used to evaluate the second order statistics of the received signal.

The level-crossing rate $N(r)$ is defined as the rate at which a stochastic process crosses a specified signal level r in a positive going direction. The number of level-crossings per second is given by [1]

$$N(r) = \int_0^\infty \dot{x} p(r, \dot{x}) d\dot{x}, \qquad r \geq 0 \tag{3.31}$$

where $\dot{x}$ is the time derivative or the slope of $x(t)$ and $p(r, \dot{x})$ is the joint probability density function of the specified level r. Here, it follows that the envelope $\zeta(t) = |\mu(t)|$ tends to the Rayleigh distribution $p_\zeta(r)$. The theoretical term of the LCR for such a Rayleigh fading channel is defined as [1]

$$N_\zeta(r) = \sqrt{\frac{\beta}{2\pi}} \cdot \frac{r}{\psi_0} \cdot e^{-\frac{r^2}{2\psi_0}}, \tag{3.32}$$

where

$$\beta = -\ddot{\psi}_0 - \frac{\dot{\phi}_0^2}{\psi_0}. \tag{3.33}$$

The quantities $\ddot{\psi}_0$, $\dot{\phi}_0^2$, and ψ_0 can be obtained from (3.28), (3.29), and (3.30). Therefore, the corresponding LCR of the evolving ACF in the previous section can be obtained.

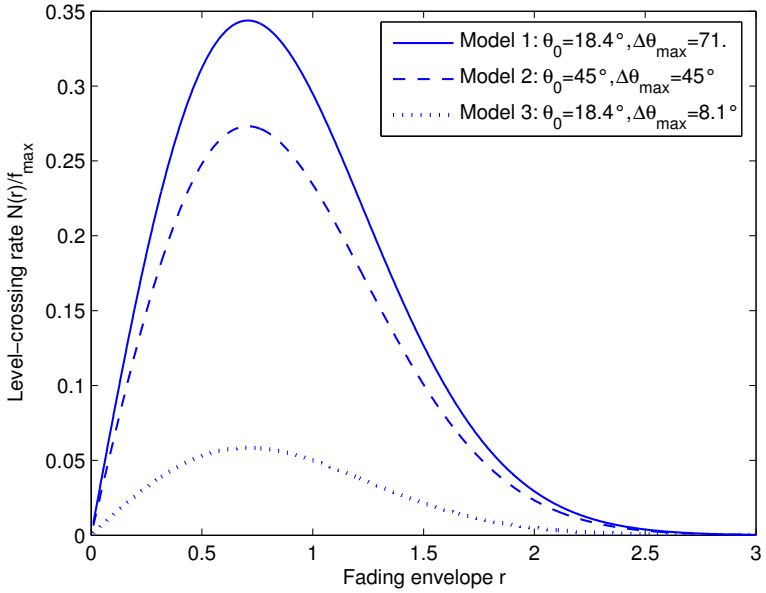

Figure 3.8: The normalized LCR of the fading envelope for different lengths of a cluster with different θ_0 and $\Delta\theta_{\max}$ ($h/D = 0.3$, $f_{R_{\max}} = 41.7$ Hz, $\sigma_0 = 0.5$)

Figure 3.8 shows the normalized LCR ($N(r)/f_{R_{\max}}$) under the assumption that the transmitter is fixed and the receiver is on the move with $v_R = 50$km/h in the direction of $\theta_v = 120^o$ with different lengths and positions of a cluster. It is readily apparent in Fig. 3.8, the LCR $N(r)$ of the third model with $l = 5$, $\alpha_0 = \pi/2$, and $\Delta\alpha_{\max} = \pi/4$ is greatly decreased compared to the other two models.

Since the relation between the distance from transmitter or receiver to the roadside (h) and the space between the mobiles (D) influence the PDF of the angular spread and path lengths, the comparison of three different values of h/D is now considered and plotted in Fig. 3.9.

As a result, when comparing the graphs in Fig. 3.9, the LCR of the relationship $h/D = 0.1$ is the lowest. It indicates that the smaller a relationship between h/D, the smaller the LCR is.

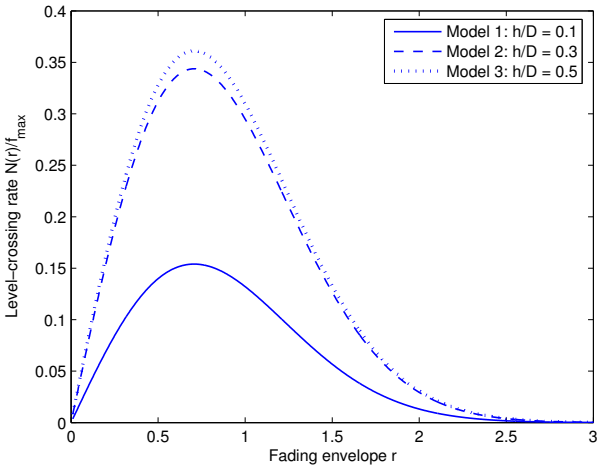

Figure 3.9: The normalized LCR of the fading envelope for different values of h/D, ($f_{R\max} = 41.7$ Hz, $\sigma_0 = 0.5$)

Next, the direction of motions of the transmitter and receiver are taken into account with the same given values as in the last section. Figure 3.10 illustrates the normalized LCR for mobile-to-mobile channel based on the geometrical street model.

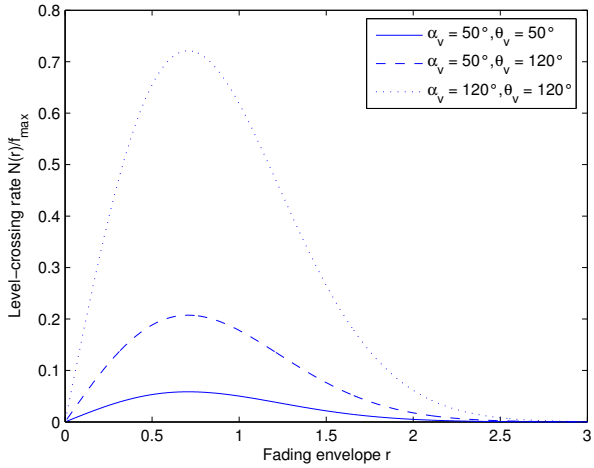

Figure 3.10: The normalized LCR of the fading envelope for mobile-to-mobile channel with different direction of motions ($h/D = 0.3$, $f_{T\max} = f_{R\max} = 41.7$ Hz, $\sigma_0 = 0.5$)

As it can be seen from Fig. 3.10, the LCR is greatly increased, when the mobiles move apart from each other. It shows that the further they move away from each other, the greater the LCR is.

3.5 Average Duration of Fades

The ADF characterizes the severity of the fading, i.e., the average length of the duration while the channel amplitude is below a level r. The ADF is defined by

$$T(r) = \frac{F_\zeta(r)}{N_\zeta(r)}, \tag{3.34}$$

where

$$F_\zeta(r) = \int_0^r p_\zeta(x)dx \tag{3.35}$$

denotes the cumulative distribution function of the process $\zeta(t)$. Then, the ADF can be expressed as

$$T_\zeta(r) = \sqrt{\frac{2\pi}{\beta}} \cdot \frac{\psi_0}{r} \left(e^{\frac{r^2}{2\psi_0}} - 1 \right), \qquad r \geq 0, \tag{3.36}$$

where the parameter β and ψ_0 are given by (3.33) and (3.30), respectively. Hence, the ADF is also based on the resulting ACF. For the simplified case that the transmitter is fixed and the receiver is moving with the same specified quantities of v_R and θ_v as previously, the normalized ADF $T_\zeta(r) \cdot f_{R_{\max}}$ can be plotted in Fig. 3.11 due to different lengths and positions of a cluster.

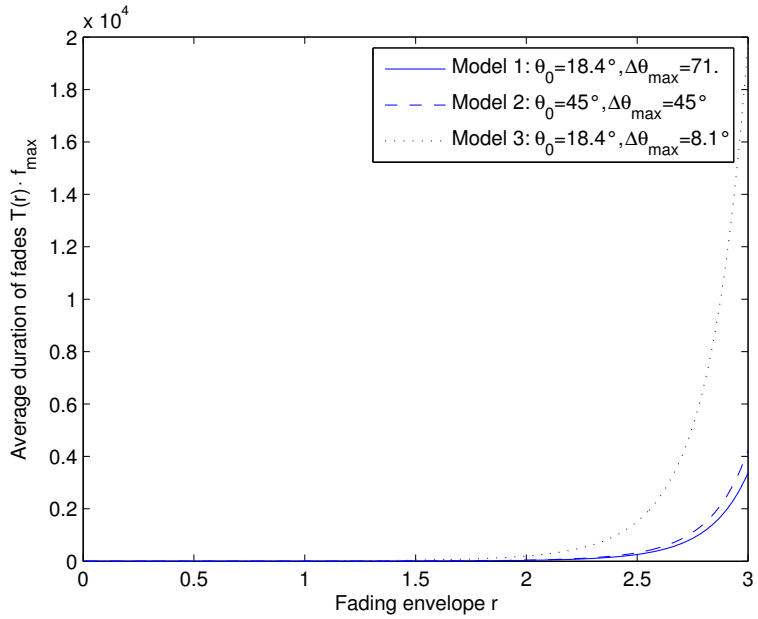

Figure 3.11: The ADF of the fading envelope for various values of l ($h = 5, D = 15, f_{R_{\max}} = 41.7$ Hz, $\sigma_0 = 0.5$)

As it is shown in Fig. 3.11, the ADF of the third model is increased, whereas the LCR of this model is greatly decreased in Fig. 3.8. Furthermore, the ratio of h/D is once again considered with the same given parameters as in Fig. 3.4 and illustrated in Fig. 3.12.

This indicates that the smaller a relationship between h/D, the greater the ADF is. That is the exact opposite result of that the LCR presented in the previous section.

The next investigation is the comparison of the ADF between different direction of motions of the mobiles with the same variables as the one shown in Fig. 3.7 and 3.10. The results of this analogy are plotted in Fig. 3.13. It is shown that the closer the transmitter and the receiver move to each other, the more the ADF increases.

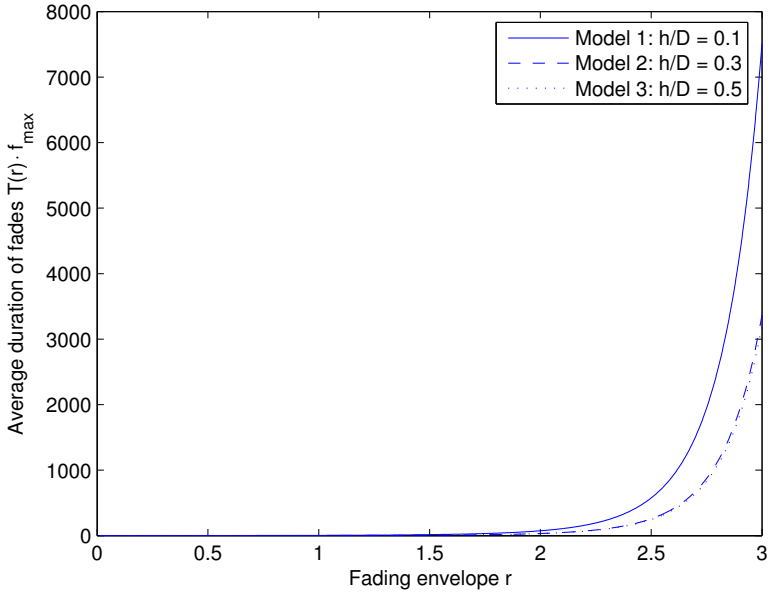

Figure 3.12: The ADF of the fading envelope for various values of h/D, ($f_{R_{\max}} = 41.7$ Hz, $\sigma_0 = 0.5$)

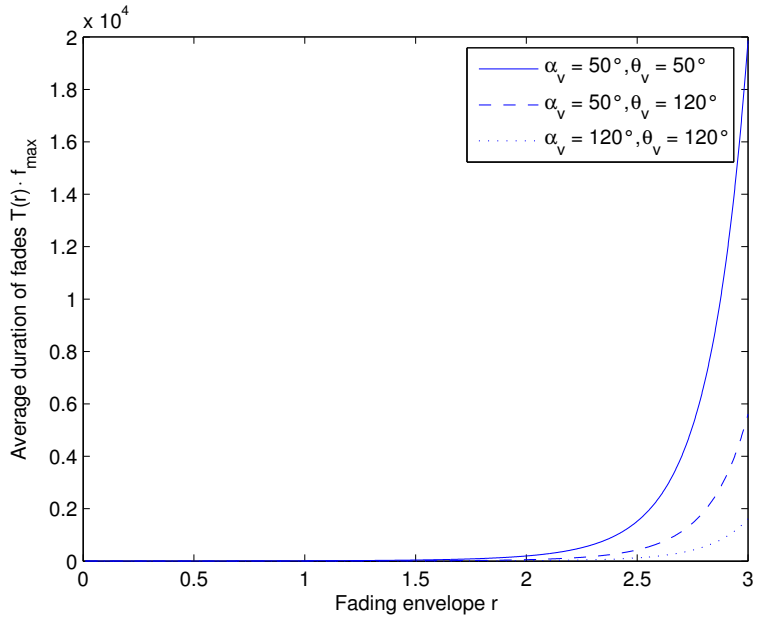

Figure 3.13: The normalized ADF of the fading envelope for mobile-to-mobile channel with different direction of motions,($h/D = 0.3$, $f_{T_{\max}} = 41.7$ Hz, $f_{R_{\max}} = 41.7$ Hz, $\sigma_0 = 0.5$)

In this chapter, I have introduced a statistical geometrical street model which assumes that the transmission undergoes only one bounce going from the transmitter to the receiver and that the scatterers are located uniformly within a cluster between the transmitter and the receiver. The statistical properties, i.e., the PDF of AOA, the Doppler PSD, the ACF, the LCR, and the ADF of the received signal are investigated enhanced by various parameters, e.g., the size and position of a cluster, h/D, and the direction of motions. The correctness of the derivations will be verified by simulations, which will be described in the next chapter.

Chapter 4

Simulation Model

The simulation is very important for the design of mobile-to-mobile radio channels, as it proves the correctness of the analytical model. In [19], the simulation of Rayleigh-faded SISO mobile-to-mobile channel is described with the development of sum-of-sinusoids. In [3], the simulation model of MIMO mobile-to-mobile fading channel is derived for the two-ring scattering model, which is researched for the propagation environment around the moving transmitter and receiver in urban and suburban areas. In this chapter, a stochastic simulation model and the corresponding deterministic simulation model are introduced for the street model.

Generally, simulation models for mobile radio channels are in progress of using at least two colored Gaussian noise processes. There are two fundamental methods for design of colored Gaussian noise processes: the *filter method* and the *sum of sinusoids method* [1] as shown in Fig. 4.1 and 4.2.

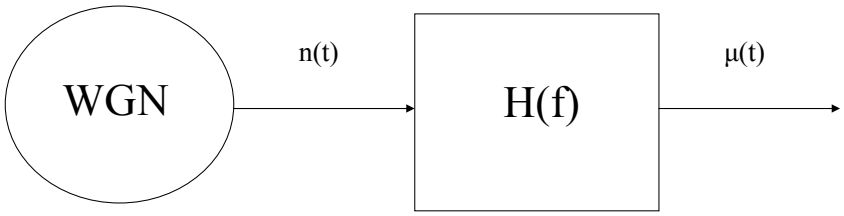

Figure 4.1: The filter method for colored Gaussian noise processes

The simulation model of this work is based on the sum of sinusoids method. The sum of sinusoids principle is a method to model Gaussian noise with given correlation properties and coming more into use in mobile communications. A colored Gaussian noise process is approximated by a finite sum of weighted harmonic functions, where c_n, f_n, θ_n, and N denote Doppler coefficients, Doppler frequencies, Doppler phases, and the number of expo-

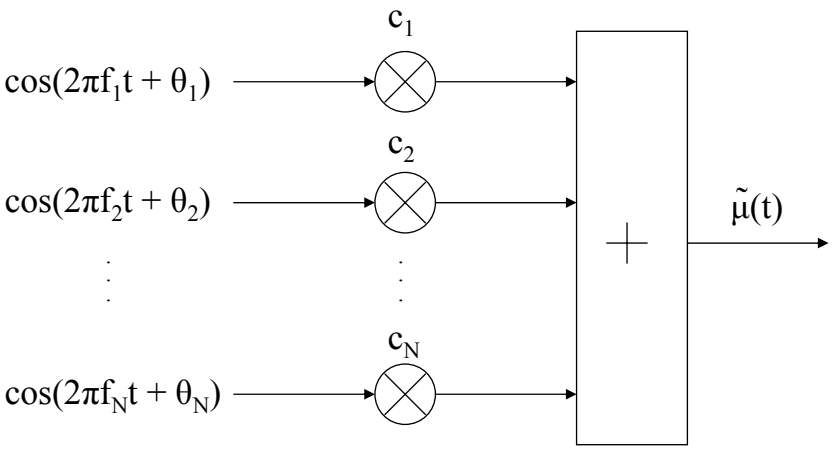

Figure 4.2: The sum of sinusoids method for colored Gaussian noise processes

nential functions, respectively. By applying the concept of deterministic channel modeling, a simulation model can be derived in three steps:

- Derivation of a stochastic simulation model from the analytical by the use of a finite number of N
- Derivation of the corresponding deterministic simulation model from the stochastic simulation model by fixing all model parameters
- Computation of deterministic simulation model parameters by using appropriate optimization algorithm, such as L_p-Norm method to the stochastic analytical model

At the end of this chapter, the simulation results are presented in comparison with the analytical model.

4.1 Stochastic Simulation Model

The relationships between analytical models, stochastic simulation models, and deterministic simulation models are shown in Fig. 4.3. A stochastic simulation model is obtained by using a finite number of exponential functions N and can be defined by

$$\hat{\mu}(t) = \sum_{n=1}^{N} c_n e^{j(2\pi f_n t + \theta_n)}, \tag{4.1}$$

where the coefficients c_n and the frequencies f_n are constant and the phases θ_n are uniformly distributed random variables in the interval $(0, 2\pi]$. Since c_n, f_n, and θ_n are kept constant during the simulation in this work, the deterministic simulation model is considered and presented in the next section.

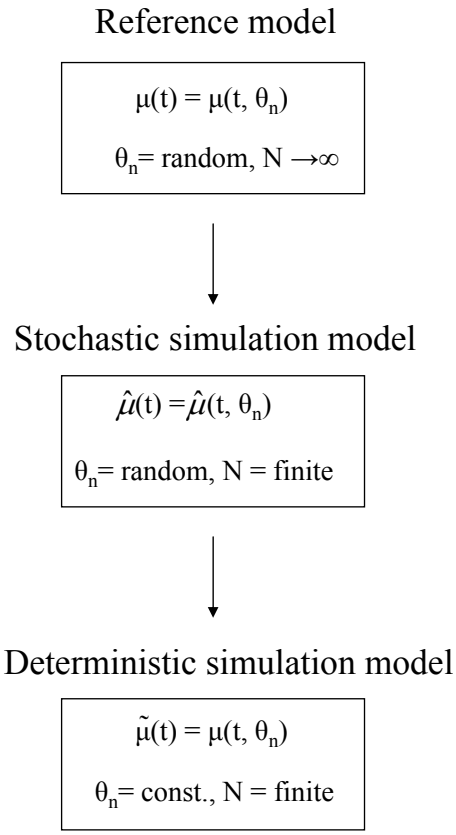

Figure 4.3: Relationship between a reference model, stochastic simulation model, and deterministic simulation model

4.2 Deterministic Simulation Model

As you can see in Fig. 4.3, the difference from the stochastic simulation model is that all model parameters in the deterministic simulation model are specified, inclusive the phases θ_n. In this section, the statistical properties of the deterministic simulation model are investigated and should be fitted as close as possible to the analytical model. The deterministic process can be expressed as

$$\tilde{\mu}(t) = \sum_{n=1}^{N} c_n e^{j(2\pi f_n t + \theta_n)}, \tag{4.2}$$

where N stands for the number of exponential functions. It is mentionable that the parameters c_n, f_n, and θ_n are computed during the simulation setup period by the L_p-norm method described in the next section. Later on, these quantities are known and kept constant, while the simulation runs. This shows that $\tilde{\mu}(t)$ can be considered as a deterministic

function. The autocorrelation function ACF is considered as

$$\tilde{r}_{\mu\mu}(\tau) = \sum_{n=1}^{N} c_n^2 e^{j2\pi f_n \tau}, \tag{4.3}$$

where

$$c_n = \sigma_0 \sqrt{\frac{2}{N}}. \tag{4.4}$$

In this work, the coefficients c_n are defined by (4.4), therefore, the performance of $\tilde{r}_{\mu\mu}(\tau)$ is totally depending on f_n. The quantity f_n is needed to be fitted in the simulation model and the analytical model. The discrete f_n can be determined so, that the ACF of the deterministic process $\tilde{r}_{\mu\mu}(\tau)$ gives an optimal estimation of the ACF of the stochastic process $r_{\mu\mu}(\tau)$ within a proper time interval. To minimize the difference between the ACF of deterministic and stochastic process, the L_p-norm can be applied as well as other minimization algorithms [1].

4.3 Parameter Computation Method

The parameter computation method L_p-norm is described in detail in [1]. As the autocorrelation function $\tilde{r}_{\mu\mu}(\tau)$ depends on the Doppler coefficient c_n and the discrete Doppler frequency f_n, according to (4.3), this method enables to find proper values for the discrete Doppler frequencies f_n. Since the Doppler coefficients c_n are fixed and given by (4.4), only optimal values for the discrete Doppler frequencies f_n have to be found numerically by minimizing the error function $E_{r_{\mu\mu}}^{(p)}$ between $r_{\mu\mu}(\tau)$ and $\tilde{r}_{\mu\mu}(\tau)$, which is for the L_p-norm defined as following:

$$E_{r_{\mu\mu}}^{(p)} = \left\{ \frac{1}{\tau_{\max}} \int_0^{\tau_{\max}} |r_{\mu\mu}(\tau) - \tilde{r}_{\mu\mu}(\tau)|^p \, d\tau \right\}^{1/p}, \tag{4.5}$$

where $p = 2$ in this case. The parameter $\tau_{\max}$ denotes the time interval over which the approximation $r_{\mu\mu}(\tau)$ is of interest and can approximately be $\tau_{\max} \approx N/(2f_{\max})$. The autocorrelation function $\tilde{r}_{\mu\mu}(\tau)$ of the deterministic process given by (4.3) will be suited to the autocorrelation function $r_{\mu\mu}(\tau)$ of the analytical model in (3.20) as close as possible.

4.4 Numerical Results

Random variables play an important role in the deterministic simulation model. Therefore, random variables of a certain probability density function are needed to simulate the different statistical properties of the channel model, such as the Doppler PSD. The used

algorithm to determine arbitrary PDF's will be briefly described below.

To generate random variables of a specific PDF, its cumulative distribution function (CDF) is needed. Furthermore, for a uniformly distributed random variable U, which can be easily generated in MATLAB, the probability of a realization u_i $F(u_i) = u_i$ holds. As it is shown in Fig. 4.4, the probability $F(u_i)$ of the uniformly distributed random variable U between [0,1] is the same as the probability $F(x_i)$ of one realization x_i of a random variable U with an arbitrary chosen CDF, i.e., $F(u_i) = F(x_i)$. Subsequently, the realization x_i can be calculated by the inverse CDF $(F^{-1}(u_i))$.

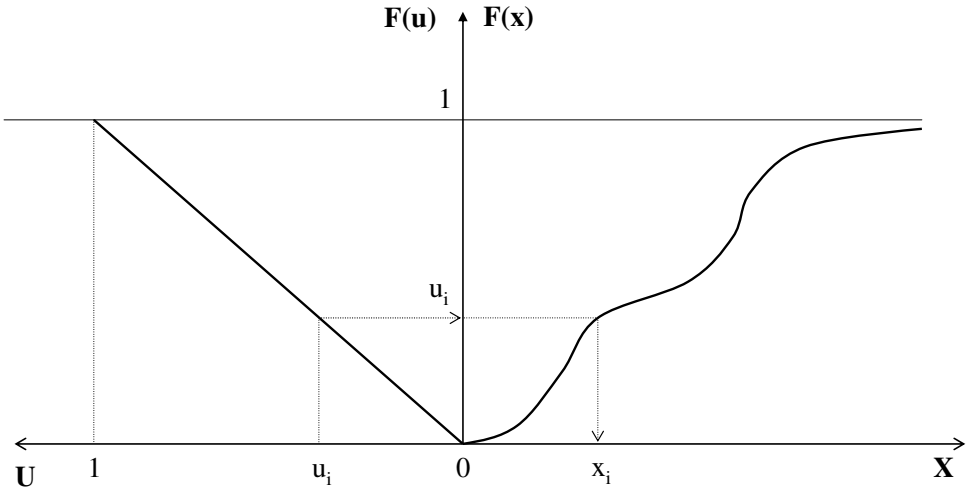

Figure 4.4: Relationship between the probability density function and its cumulative distribution function

The analytical rearrangement of the inverse CDF can be very difficult. However, for the deterministic simulation model, the CDF is discret and exists as a vector of $i = 0, 1, 2..., N$ elements, each with one probability for the realization x_i. The wanted realization x_i, or the inverse of the CDF $F^{-1}(x_i)$, is then the i^{th} element from the CDF vector, which matches first the probability $F(u_i)$.

The derivation for the PDF of the angular spread at the receiver $p_{\Delta\theta}(\Delta\theta)$ is now verified by the simulation. The case, that the transmitter is fixed and the receiver is on the move with the speed $v_R = 50$km/h and the $\theta_v = 120^o$, is again considered with the same specified parameters as those for the fist model in Fig. 3.1. It should be noted that the AOD α and the AOA θ are limited in the interval $(-\pi/2, \pi/2)$. The discrete $\Delta\theta$ at the receiver is calculated by (3.1) for each scatterer within the angle of spreading $\Delta\alpha$ at the transmitter. The simulated histogram of the angular spread $\Delta\theta$ at the receiver is plotted compared to the analytical resultin Fig. 4.5, whereas 50 bins were used.

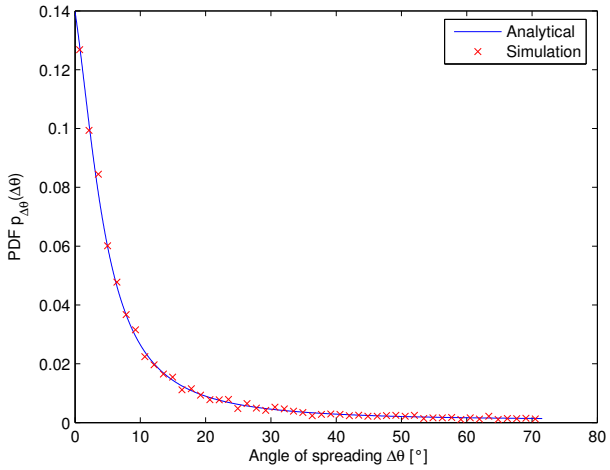

Figure 4.5: The theoretical PDF of the angular spread $\Delta\theta$ compared to the simulation result ($h = 5, l = 15, D = 15, \alpha_0 = \pi/2, \Delta\alpha_{\max} = 71.7^o$)

The simulated PDF of the angular spread $p_{\Delta\theta}(\Delta\theta)$ and the analytical one fit perfectly as can be seen in Fig. 4.5. Next, the derivation for the Doppler PSD is examined and normalized by σ_0^2 for the case that the transmitter obtains $v_T = 0$ and the receiver moves with $v_R = 50$ in the direction of $\theta_v = 120^o$. The discrete Doppler frequencies f are calculated by (3.10) for each bin. This cluster of scatterers maintains the same length as the distance between the transmitter and the receiver, i.e., the maximum possible length. The simulated histogram of the normalized Doppler PSD/σ_0^2 is plotted in Fig. 4.6, whereas the simulated frequency vector has been again divided into 50 bins.

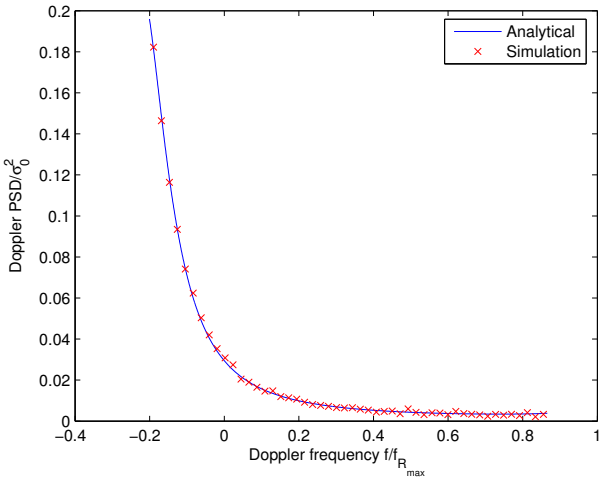

Figure 4.6: The Doppler PSD in comparison with the analytical model ($h = 5, D = 15, f_{R_{\max}} = 41.7$ Hz, $\sigma_0 = 0.5$)

As it is shown in Fig. 4.6, the simulation result of the Doppler PSD is suitable to the analytical model. Furthermore, the simulation of the absolute value of the ACF $r_{\mu\mu}(\tau)$ is investigated by evaluating (4.3) and minimizing the error of (4.5) to find optimal Doppler frequencies f_n with the L_p-norm method, since the coefficients c_n is already achieved by (4.4). The discrete Doppler frequencies are then available for the realization of the deterministic simulation model. As starting values of the discrete Doppler frequencies f_n $(n = 1, 2, ...N)$, random frequency values between f_l and f_u have been taken into account. The upper limit of the integral in (4.5) is defined by the relation $\tau_{\max} = N/(2f_{\max})$. Following optimization results are based on the L_p-norm $E^{(p)}_{r_{\mu\mu}}$ with $p = 2$.

The result of the simulation compared to the analytical model is shown in Fig. 4.7 for the case that the transmitter is fixed and the receiver is moving with $v_R = 50$km/h and $\theta_v = 120^o$. Figure 4.7 gives an impression of the behavior of the ACF for $N = 30$ in this case.

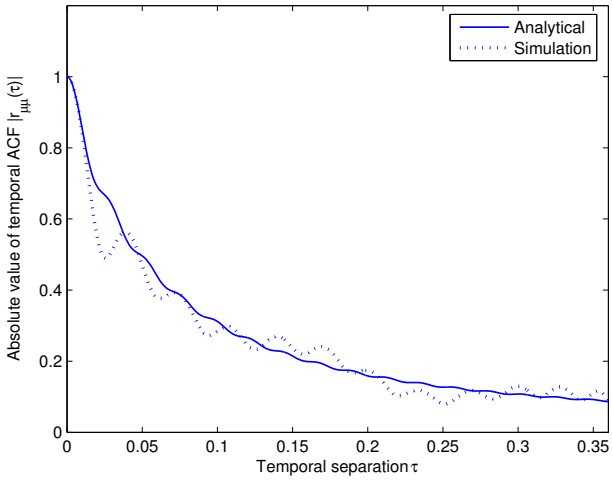

Figure 4.7: The absolute value of the ACF of the simulation model in comparison with the analytical model ($h = 5, D = 15, f_{R_{\max}} = 41.7$ Hz, $\sigma_0 = 0.5, p = 2, N = 30$)

As mentioned before, different direction of motions of the transmitter and the receiver have an impact on the ACF. After minimization (4.5) with the L_p-norm method, the optimized discrete Doppler frequencies are obtained. The simulation of the ACF is carried out in the same way as described earlier. The ACF of the stochastic process $r_{\mu\mu}(\tau)$ in (3.21) and deterministic process $\tilde{r}_{\mu\mu}(\tau)$ in (4.3) are used. The various directions of motions of the mobiles are now taken into consideration. The simulation results for the ACF is illustrated in Fig. 4.8. The results of the analytical model is also presented in this figure.

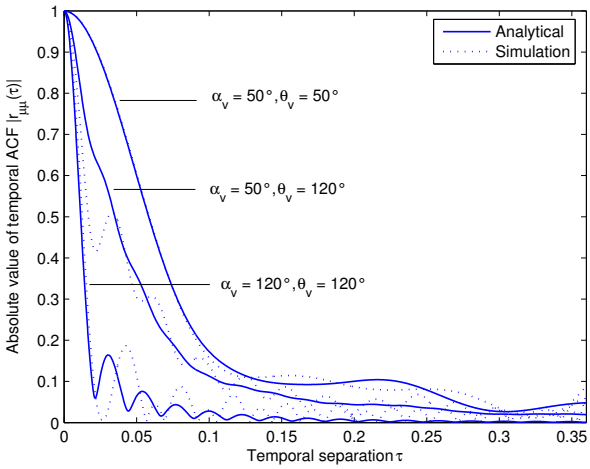

Figure 4.8: The absolute value of the ACF of the simulation model in comparison with the analytical model for mobile-to-mobile communication due to different direction of motions ($h = 5, D = 15, f_{T_{\max}} = f_{R_{\max}} = 41.7$ Hz, $\sigma_0 = 0.5, p = 2, N = 30$)

Figure 4.9 illustrates the simulation result of the LCR and the ADF compared to the analytical result. It indicates that the results of the simulation and analytical model does not fit perfectly with each other.

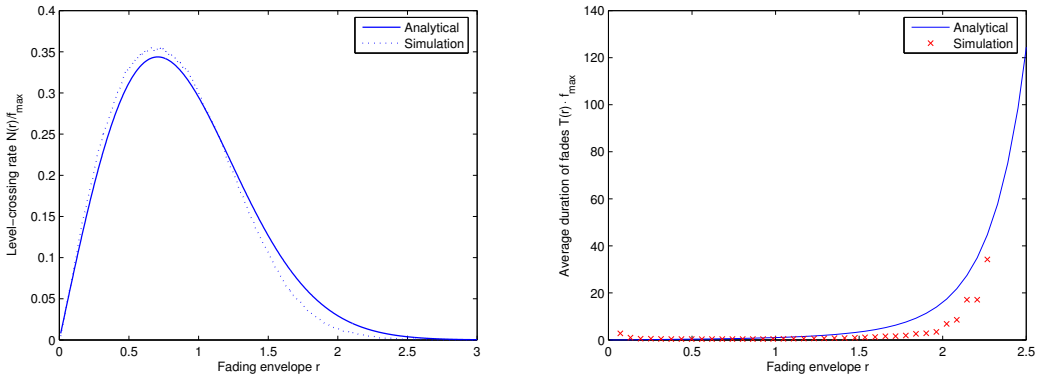

(a) (b)

Figure 4.9: (a) the LCR and (b) the ADF of the simulation model in comparison with the analytical model ($h = 5, D = 15, f_{R_{\max}} = 41.7$ Hz, $\sigma_0 = 0.5, p = 2, N = 30$)

Chapter 5

Extensions of the Street Model

So far, the geometrical street model for mobile-to-mobile single-input single-output (SISO) systems has been introduced. In any wireless channel, scatterers are not distributed uniformly throughout the whole propagation area, but rather occur in clusters. Clusters of scatterers correspond to buildings in urban environments and hills or mountains in rural environments. Due to the improvements of mobile communication systems, the enhancement of capacity, quality, and data rates becomes an important role. Therefore, the development of multielement antennas is taken into account. In this chapter, the extensions of the street model are investigated. These include several clusters of scatterers, frequency-selective channel, and multiple-input multiple-output (MIMO) mobile-to-mobile channel.

5.1 Multiple Clusters of Scatterers

In scattering environment, the propagation paths to the receiver will arrive from a certain angular spread of directions. This means that the signal is scattered and reflected from objects in the environment and that components of the signal at the receiver are spread out over a longer period of time. In general, the signals at the receiver are from different directions due to multipath propagation. An important property, which characterizes the channel and receiver algorithms, is the angle of arrival (AOA) θ. The main arrival direction hardly changes as the channel changes rapidly due to the movement of mobiles and environments. Another property which determines the quality of the communication link is the angular spread $\Delta\theta$. Due to the geometrical street model, a certain angular spread occurs at the receiver, which is referred to as a part of the representation of the AOA.

In Chapter 2, an angular spread results from a cluster of scatterers. The signal wave is propagated from a scatterer directly to the receiver without interaction with the other scatterers in the cluster. A cluster is a geometrically distributed group of scatterers. Essentially, the signal may come from several clusters which will be analyzed in this chapter.

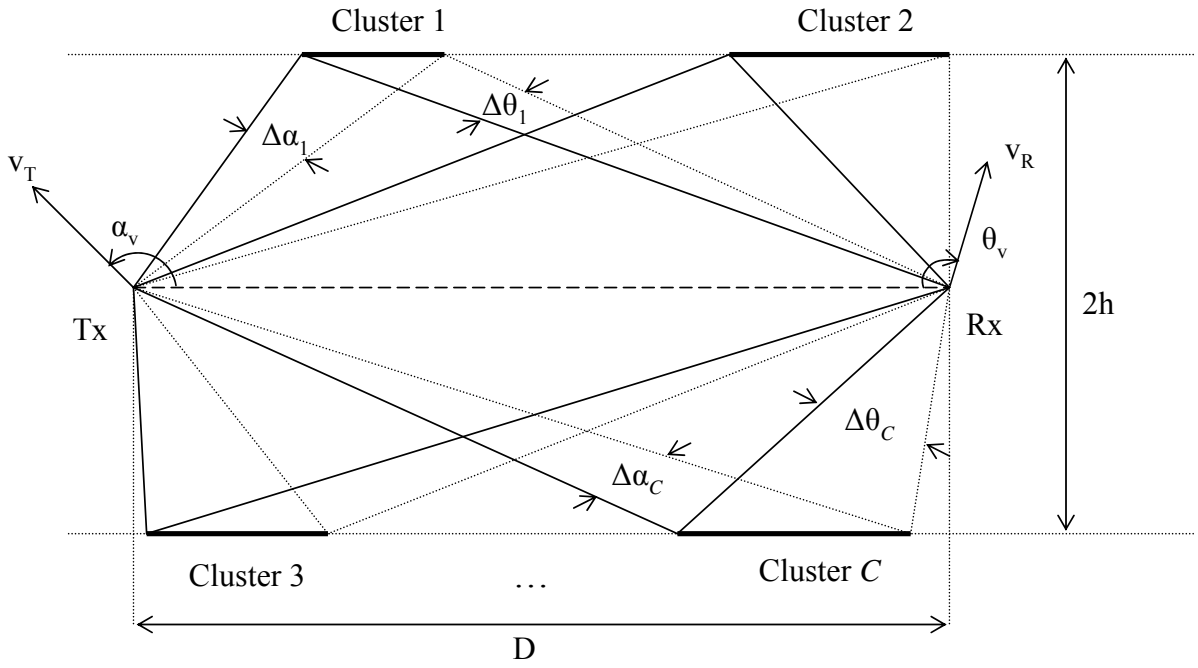

Figure 5.1: Geometrical street model with several clusters of scatterers

In this section, a radio environment with $\mathcal{C}$ clusters is considered. Figure 5.1 shows the geometrical model for a mobile-to-mobile radio channel with several clusters of scatterers based on the street model. The subscript $(\cdot)_c$ $(c = 1, 2, ..., \mathcal{C})$ is used to identify the particular cluster of scatterers.

5.1.1 Statistical Properties

At the beginning of an analysis of statistical properties for multiple clusters, the signal for this channel was specified by the use of the superposition principle. This implies that the signal at the receiver is the sum of the signals which are caused by the individual clusters of scatterers. Thus, the consideration of the performance of each cluster enables the analysis of multiple clusters by summing the result of each cluster to find the complete result of several clusters. For instance, the probability density function (PDF) of the angular spread $p_{\Delta\theta}(\Delta\theta)$ could be defined by

$$p_{\Delta\theta}(\Delta\theta) = \sum_{c=1}^{\mathcal{C}} w_c p_{\Delta\theta_c}(\Delta\theta_c), \tag{5.1}$$

where w_c is a weighting factor for the cth cluster of scatterers. Due to $\int_{-\infty}^{\infty} p(x)dx = 1$,

the constraint $w_c = 1/c$ was established. This way of the analysis for multiple clusters did not turn out to be correct. An alternative solution is to generate random variables of the specified PDF of the angular spread $p_{\Delta\alpha}(\Delta\alpha)$, described in Section 4.4, and associate these variables with the geometrical relation between $\Delta\alpha$ and $\Delta\theta$.

The statistical properties of a single cluster of scatterers for the street model are analyzed in Chapter 3. From the theory developed in this chapter, it is well-known that a certain multiple clusters shape of the $p_{\Delta\alpha}(\Delta\alpha)$ at the transmitter results in a proper $p_{\Delta\theta}(\Delta\theta)$. The specification of initial angles of departure α_0 together with boundary angles of departure α_b define the length and position of each cluster.

For ease of analysis, the transmitter is firstly considered to be fixed and the receiver moves with the speed v_R in the direction of θ_v. The comparison of a single cluster and several clusters of scatterers are taken into account into two following models:

- Model 1: $l = 15$, $\alpha_0 = \frac{\pi}{2}$, $\alpha_b = 18.4^o$, $\Delta\alpha_{\max} = 71.7^o$,
  the corresponding angles $\theta_0 = 18.4^o$ and $\Delta\theta_{\max} = 71.7^o$
- Model 2: $l_c = [3 \quad 5 \quad 3]$, $\alpha_0 = [22.6^o \quad 45^o \quad \frac{\pi}{2}]$, $\alpha_b = [18.4^o \quad 26.6^o \quad 59^o]$,
  the corresponding angles $\theta_0 = [59^o \quad 26.6^o \quad 18.4^o]$

The quantity l_c characterizes the length of the cth cluster, in this case, $c = 3$. For the comparison of these analytical models, the performance curves for statistical properties are plotted in Fig. 5.2. These include the PDF of the angular spread at the receiver $p_{\Delta\theta}(\Delta\theta)$, the Doppler power density function (PSD) $S_{\mu\mu}(f)$, the autocorrelation function (ACF) $r_{\mu\mu}(\tau)$, and the level-crossing rate (LCR) $N(r)$.

Figure 5.2(a) and 5.2(b) illustrate that the curves of the first and the second model have the same shape, but the curve of the first model lies beneath the second one. The reason for this is that the area below the curves of these two models has to be the same and equal to one due to the fact that $\int_{-\infty}^{\infty} p_{\Delta\theta}(\Delta\theta) = 1$.

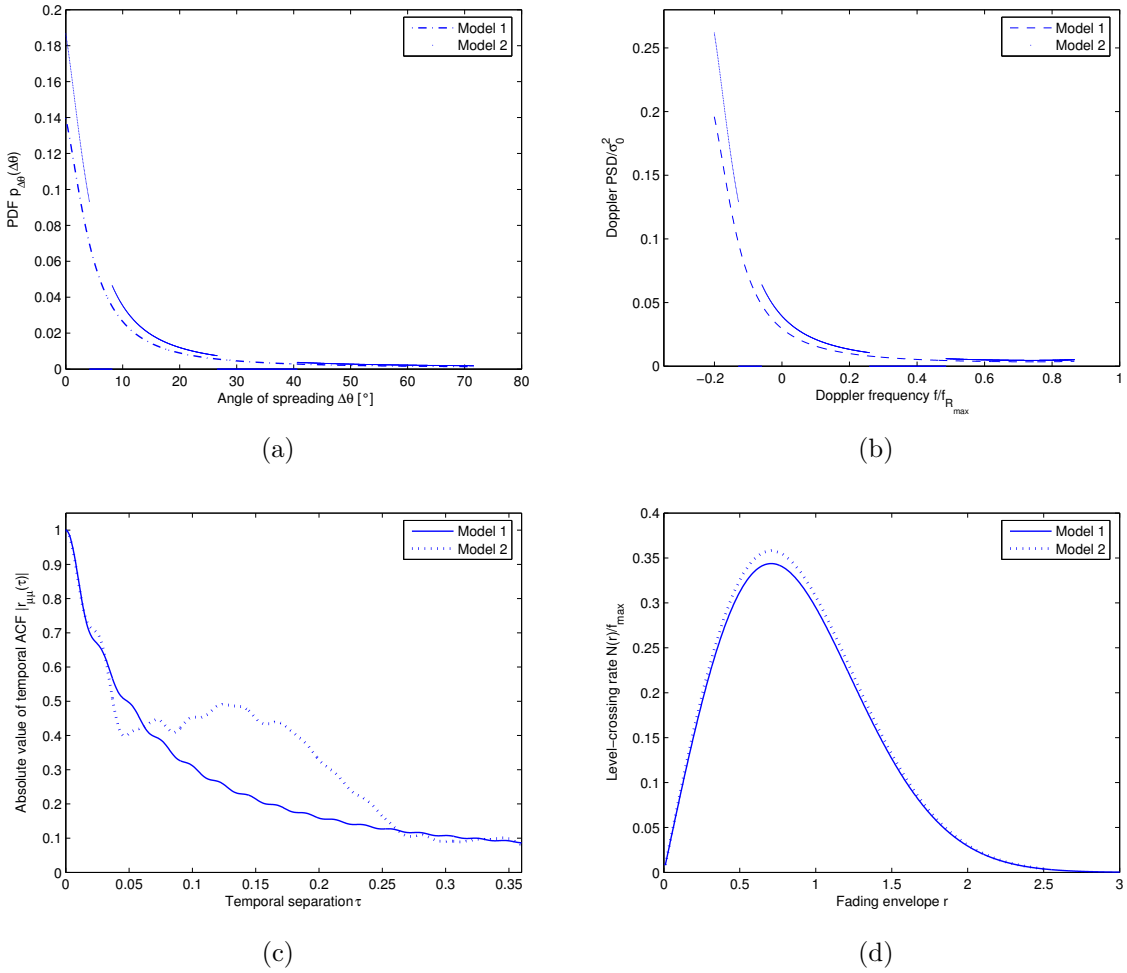

(a) (b) (c) (d)

Figure 5.2: Illustration of statistical properties (a) probability density function of the angular spread $p_{\Delta\theta}(\Delta\theta)$, (b) normalized Doppler power spectral density function $S_{\mu\mu}(f)/\sigma_0^2$, (c) absolute value of autocorrelation function $|r_{\mu\mu}(\tau)|$, and (d) normalized level-crossing rate $N(r)/f_{\max}$ for a single cluster and multiple clusters of scatterers ($h = 5, D = 15, \theta_v = 120^o$, $f_{R_{\max}} = 41.7$ Hz, and $\sigma_0 = 0.5$)

It should also be observed that the transmitter and the receiver are moving in the directions shown in Fig. 5.1 with v_T and v_R, respectively, by reason of mobile-to-mobile communication system. The direction of motions of the transmitter and the receiver affects the ACF, LCR, and ADF of the channel model. Fig. 5.3 illustrates these statistical properties of three clusters of scatterers in comparison with a single cluster of scatterers with the same specified parameters as above. The transmitter (receiver) is on the move in the direction of $\alpha_v = 120^o$ ($\theta_v = 120^o$) with $v_T = 50$km/h ($v_R = 50$km/h).

As a result shown in Fig. 5.3(a), the ACF of both models are greatly decreased at the beginning and shortly afterward the amplitude of the second model is higher. Hence, the LCR of the first model is increased greater than the second one, therefore, the ADF of the first model is less than the second one.

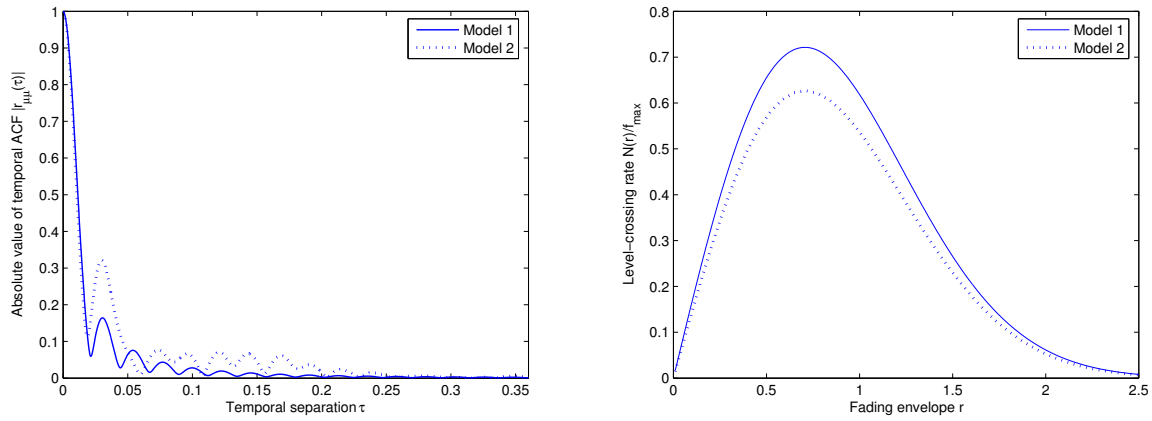

(a)

(b)

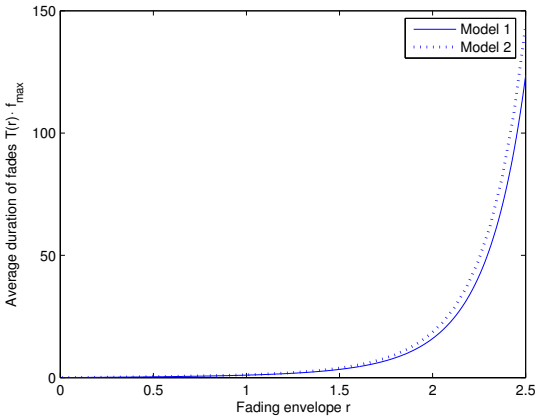

(c)

Figure 5.3: Statistical properties (a) absolute value of autocorrelation function $|r_{\mu\mu}(\tau)|$, (b) normalized level-crossing rate $N(r)/f_{\max}$, and (c) normalized average duration of fades for multiple clusters of scatterers when the both mobiles are on move compared to a cluster of scatterers ($h = 5, D = 15, f_{T_{\max}} = f_{R_{\max}} = 41.7$ Hz, and $\sigma_0 = 0.5$)

5.1.2 Simulation Results

As the simulation is of importance for the performance of mobile communication systems, simulation results for the geometrical street model with multiple clusters are presented by the use of the concept of deterministic channel modeling described in Chapter 4.

The PDF of the angular spread $\Delta\theta$ at the receiver and the Doppler PSD for the second model (three clusters of scatterers) are verified by the simulation. The angle of departure α is uniformly distributed in each cluster. The discrete $\Delta\theta$ is given by (3.1). Thus, the discrete Doppler frequencies f are calculated by (3.10) for the case that only the receiver is on the move. The simulated histograms of the $\Delta\theta$ and the normalized Doppler frequency are plotted in Fig. 5.4 with 50 bins. The analytical results of this model are also represented in Fig. 5.4 as a comparison.

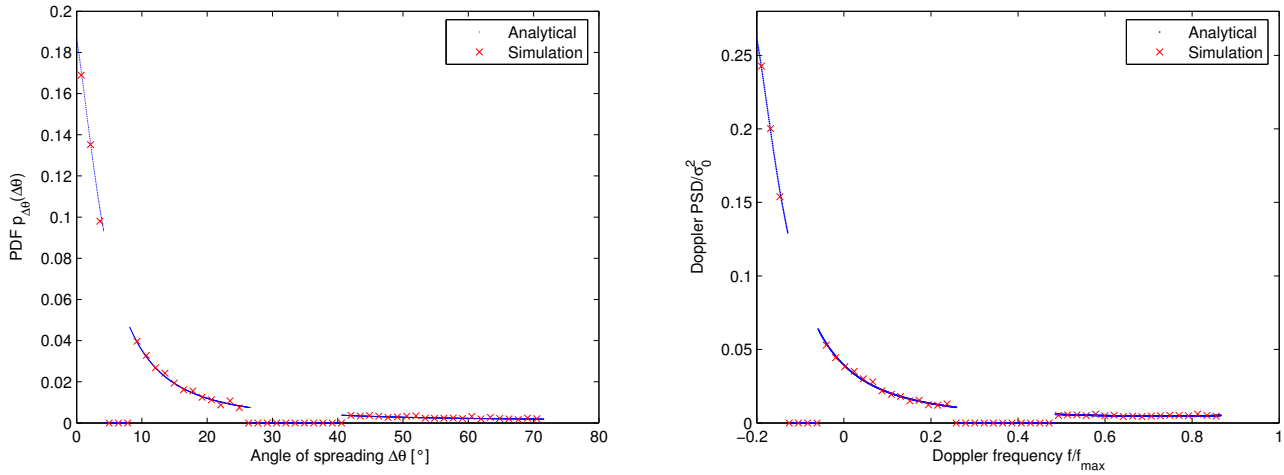

(a) (b)

Figure 5.4: (a) Probability density function of the angular spread $\tilde{p}_{\Delta\theta}(\Delta\theta)$ and (b) Doppler power density function $\tilde{S}_{\mu\mu}(f)/\sigma_0^2$ for three-cluster model ($h = 5, D = 15, v_R = 50$km/h, $f_{R_{\max}} = 41.7$ Hz, and $\sigma_0 = 0.5$)

Hence, the excellent accordance between the analytical and the simulation model of the PDF of the angular spread and the Doppler PSD for the multiple clusters of scatterers are shown in Fig. 5.4. Furthermore, the ACF of this model is also taken into account and plotted in Fig. 5.5 in comparison to the ACF of a cluster of scatterers.

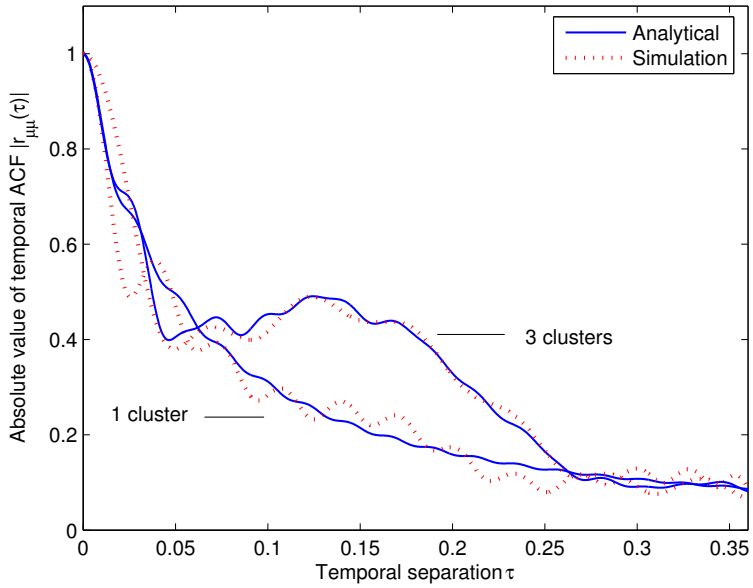

Figure 5.5: Absolute value of the autocorrelation function (ACF) of several clusters of scatterers compared to a single cluster of scatterers($h = 5, D = 15, \theta_v = 120^o$, $f_{R_{\max}} = 41.7$ Hz, and $\sigma_0 = 0.5$)

As the transmitter and the receiver are moving in the direction α_v and θ_v, respectively, the absolute value of the ACF is shown in Fig. 5.6.

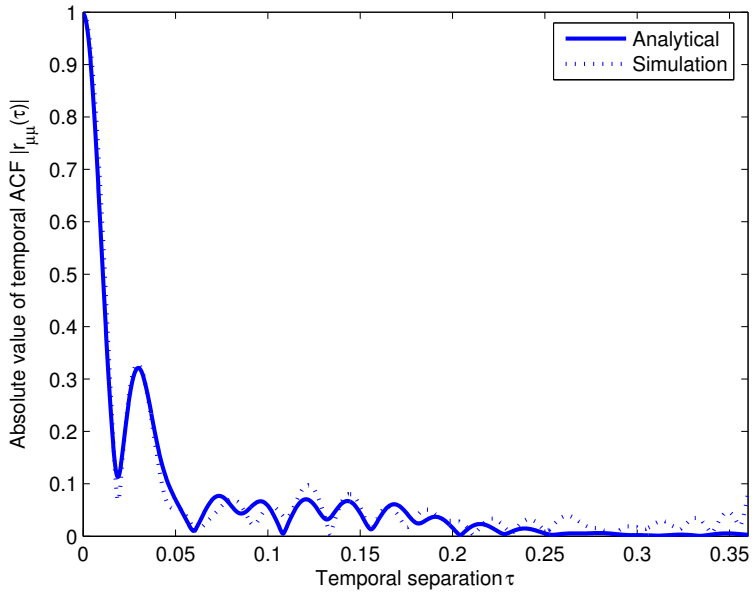

Figure 5.6: Absolute value of the autocorrelation function (ACF) of three clusters of scatterers for mobile-to-mobile systems ($h = 5, D = 15, \alpha_v = \theta_v = 120^o$, $f_{T_{\max}} = f_{R_{\max}} = 41.7$ Hz, and $\sigma_0 = 0.5$)

In this section, the performance of multiple clusters of scatterers have been analyzed and simulated as an extension of the geometrical street model. So far, the frequency-nonselective channels have been proposed. The next investigation deals with the frequency-selective geometrical street model, which will be described in the next section.

5.2 Frequency Selectivity

In mobile communications, there are many propagation paths between the transmitter and the receiver. The propagation channel is a frequency-selective channel, when the time delays of multipaths are considered. Frequency-selective fading is associated with the presence of multiple signal components, each with a different propagation delay comprising the received signal. It arises because the length of each propagation path can be defined by a frequency function.

So far, frequency non-selective fading is introduced and used when the bandwidth of the transmitted signal B_s is less than the coherence bandwidth B_c of the channel. Therefore, all frequency components of the transmitted signal undergoes the same amount of attenuation and there will be no signal distortion. A measured parameter, the so-called coherence bandwidth B_c, is the frequency range over which the channel is considered constant. When the bandwidth is increased, its spectrum extrema will be attenuated. Therefore, the channel will have a filtering effect and distort the signal. Theoretically, if $B_s > B_c$, then frequency-selective fading is experienced.

5.2.1 System Functions

In [25], Bello introduced system functions to describe linear time-variant channels, thereby the impulse response $h(\tau', t)$ is one of the four system functions. The output signal of a

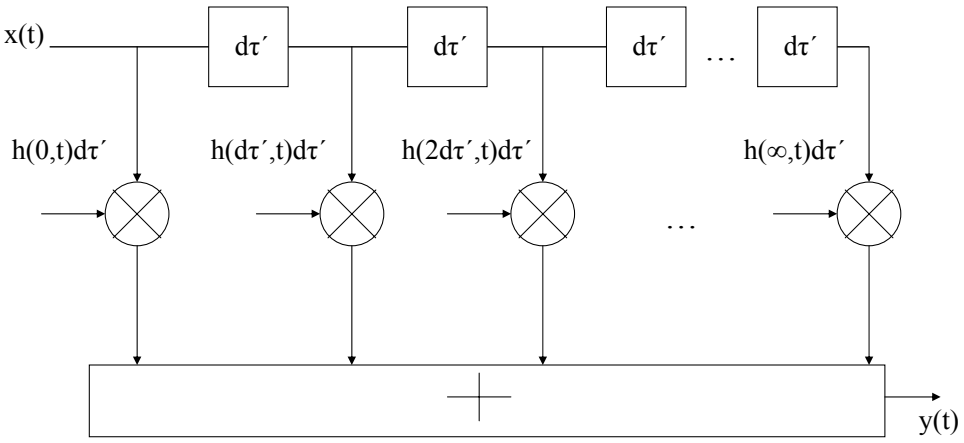

Figure 5.7: Tapped-delay-line representation of a frequency-selective and time-variant channel

time-variant channel [1] is defined by

$$y(t) = \int_0^\infty h(\tau', t)x(t - \tau')d\tau', \tag{5.2}$$

where $h(\tau', t)$ is interpreted as the response of the channel at the time t which has been excited by a unit impulse at $t - \tau'$. The output signal $y(t)$ results then as a consequence of the impulse response with an input signal $x(t)$. Figure 5.7 shows the structure of a frequency-selective channel with the time-variant impulse response $h(\tau', t)$. It is the so-called the tapped-delay-line model, where $h(\tau', t)d\tau'$ is seen to be weighted factors for a channel exciting at $(t - \tau')$. The tapped-delay-line model enables an understanding of the channel distortions with different propagation delays.

Apart from the impulse response for a time-variant system $h(\tau', t)$, the time-variant transfer function $H(f', t)$, the Doppler-variant impulse response $s(\tau', f)$, and the Doppler-variant transfer function $T(f', f)$ are also part of Bello system functions due to the multipath propagation and the Doppler effect caused by motions of the transmitter and receiver in mobile radio channels. These system functions are related in pairs by the Fourier transform as shown in Fig. 5.8.

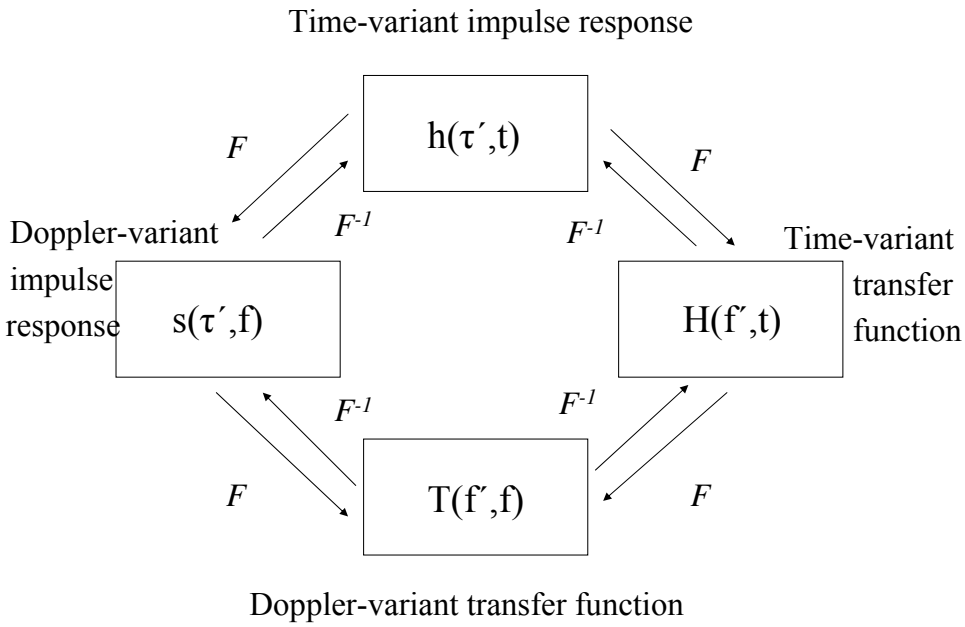

Figure 5.8: Fourier transform relationships between the Bello system functions

5.2.2 Stochastic Analytical Model

The frequency-selective street model is presented in Fig. 5.9. For the multipath propa-

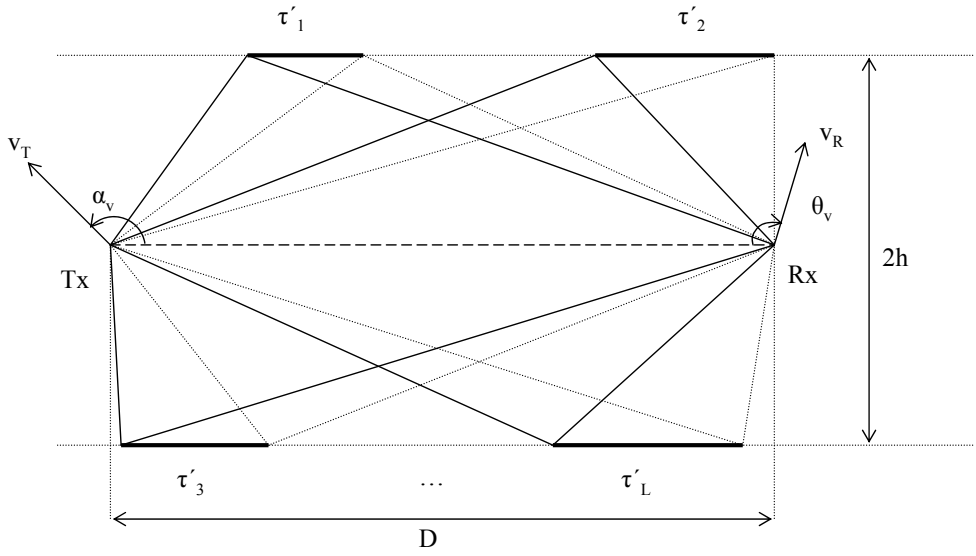

Figure 5.9: Geometrical street model with several clusters of scatterers due to frequency selectivity

gation paths of the model, not only the angles of arrival are different, but also the corresponding Doppler frequencies caused by the motion of the transmitter and the receiver due to (3.8). The path length of each wave defines the propagation delay and the average power of the wave at the receiver. Every wave in the cluster undergoes the same discrete propagation delay τ_l', where $l = 1, 2, \ldots, \mathcal{L}$, and $\mathcal{L}$ denotes the number of paths with different propagation delays. This assumption holds, as each delay τ_l' is shorter than the symbol duration in the transmitted signal.

The autocorrelation function of a stochastic process $h(\tau', t)$ at two different delays and two different times can be defined by [1]

$$r_{hh}(\tau_1', \tau_2'; t_1, t_2) = E\left\{h^*(\tau_1', t_1)h(\tau_2', t_2)\right\} \tag{5.3}$$

$$= r_{hh}(\tau_1'; \Delta t)\delta(\tau_2' - \tau_1') \tag{5.4}$$

The Fourier transform of the function above gives the scattering function. For $\Delta t = 0$, the function is referred to as the delay power spectral density and expressed as

$$S_{\tau'\tau'}(\tau') = \int_{-\infty}^{\infty} S(\tau', f)df, \tag{5.5}$$

where $S(\tau', f)$ is the scattering function with the propagation delay τ' and the Doppler frequency f. The delay power spectral density $S_{\tau'\tau'}(\tau')$ gives the power of scattering components occurring with the propagation delay τ'. The important characteristic quantities from the delay power spectral density $S_{\tau'\tau'}(\tau')$ are the average delay and the delay spread. The average delay $B^{(1)}_{\tau'\tau'}$ is the mean delay of a signal during the transmission and can be defined by

$$B^{(1)}_{\tau'\tau'} = \frac{\int_{-\infty}^{\infty} \tau' S_{\tau'\tau'}(\tau') d\tau'}{\int_{-\infty}^{\infty} S_{\tau'\tau'}(\tau') d\tau'}. \tag{5.6}$$

The delay spread $B^{(2)}_{\tau'\tau'}$ is a measure of the time spread of arriving paths through a multipath fading channel and given by

$$B^{(2)}_{\tau'\tau'} = \sqrt{\frac{\int_{-\infty}^{\infty} (\tau' - B^{(1)}_{\tau'\tau'})^2 S_{\tau'\tau'}(\tau') d\tau'}{\int_{-\infty}^{\infty} S_{\tau'\tau'}(\tau') d\tau'}} \tag{5.7}$$

The Fourier transform of the delay power spectral density is referred to as the frequency correlation function (FCF), i.e.,

$$r_{\tau'\tau'}(\upsilon') = \int_{-\infty}^{\infty} S_{\tau'\tau'}(\tau') e^{-j2\pi\upsilon'\tau'} d\tau', \tag{5.8}$$

where $\upsilon' = f'_2 - f'_1$ is a function of the frequency separation variable concerning the time-variant transfer functions $H(f'_1, t)$ and $H(f'_2, t)$. The FCF is a measure of the frequency coherence of the channel. The coherence bandwidth $B_c = \upsilon'$ can be defined by

$$|r_{\tau'\tau'}(B_c)| = \frac{1}{2} |r_{\tau'\tau'}(0)| . \tag{5.9}$$

In [25], Bello introduced the wide-sense stationary uncorrelated scattering (WSSUS) model. This model is well-known as a stochastic model for time-variant and frequency-selective mobile radio channels. It assumes that the received components with different propagation delays are statistically uncorrelated and the correlation properties of the channel are stationary. Based on the WSSUS assumption, the European working group COST 207 developed the standards for the delay power spectral density for the typical propagation environments, such as rural area, urban area, densely urban area, and hilly terrains.

5.2.3 Simulation Model

The frequency-selective simulation model is based on the principle of deterministic channel modeling. A tapped-delay line model can also be used for the simulation. The impulse response of the simulation model consists of a sum of $\mathcal{L}$ discrete propagation paths and can be defined by

$$\tilde{h}(\tau', t) = \sum_{l=1}^{\mathcal{L}} \tilde{a}_l \tilde{\mu}_l(t) \delta(\tau' - \tilde{\tau}'_l), \tag{5.10}$$

where $\mathcal{L}$ is the number of discrete propagation paths with different propagation delays, $\tilde{a}_l$ denotes the real-valued delay coefficients, and $\tilde{\tau}'_l$ represents the discrete propagation delays. Moreover, $\tilde{\mu}_l(t)$ is a complex Gaussian process and given by

$$\tilde{\mu}_l(t) = \sum_{n=1}^{N_l} c_{n,l} e^{j(2\pi f_{n,l} t + \theta_{n,l})}, \tag{5.11}$$

where N_l, $c_{n,l}$, $f_{n,l}$, and $\theta_{n,l}$ denote the number of harmonic functions, the Doppler coefficient, the Doppler frequencies, and the Doppler phases of the lth propagation path, respectively. Furthermore, it can be considered that the $\tilde{a}_l$ and the $\tilde{\tau}'_l$ determine the frequency-selective performance attributed to the effect of multipath propagation. In [1], it is shown that the scattering function $\tilde{S}(\tau', f)$ is given by

$$\tilde{S}(\tau', f) = \sum_{l=1}^{\mathcal{L}} \tilde{a}_l^2 \tilde{S}_{\mu_l \mu_l}(f) \delta(\tau' - \tilde{\tau}'_l), \tag{5.12}$$

where $\tilde{S}_{\mu_l \mu_l}(f)$ denotes the Doppler power spectral density of the deterministic process. Since $\int \tilde{S}_{\mu_l \mu_l}(f) df = 1$, the delay power spectral density function can be expressed as

$$\tilde{S}_{\tau'\tau'}(\tau') = \sum_{l=1}^{\mathcal{L}} \tilde{a}_l^2 \delta(\tau' - \tilde{\tau}'_l). \tag{5.13}$$

Thus, $\tilde{S}_{\tau'\tau'}(\tau')$ is a sum of delta functions, where the delta functions are located at $\tau' = \tilde{\tau}'_l$ and weighted by $\tilde{a}_l^2$. As the correlation function and the power spectral density function are a Fourier transform pair, the FCF $\tilde{r}_{\tau'\tau'}(\upsilon')$ of the simulation model are defined by

$$\tilde{r}_{\tau'\tau'}(\upsilon') = \sum_{l=1}^{\mathcal{L}} \tilde{a}_l^2 e^{-j2\pi\upsilon'\tilde{\tau}'_l}. \tag{5.14}$$

Substitute (5.6) and (5.7) in (5.13), the mean delay and the delay spread of the simulation model are represented by

$$\tilde{B}^{(1)}_{\tau'\tau'} = \sum_{l=1}^{\mathcal{L}} \tilde{\tau}'_l \tilde{a}_l^2 \tag{5.15}$$

$$\tilde{B}^{(2)}_{\tau'\tau'} = \sqrt{\sum_{l=1}^{\mathcal{L}} (\tilde{\tau}'_l \tilde{a}_l)^2 - \left(\tilde{B}^{(1)}_{\tau'\tau'}\right)^2}. \tag{5.16}$$

As the delay power spectral density function, the FCF, the average delay, and the delay spread totally depend on the delay coefficient $\tilde{a}_l$ and the propagation delay $\tilde{\tau}'$, the quantities $\tilde{a}_l$ and $\tilde{\tau}'$ are needed to be computed in such a way that the characteristics of the simulation model are as close as possible to those of the reference model. One method which can be

used for the computation of these two parameters is the L_p-norm method. The optimal values can be found by minimizing the following error function

$$E^{(p)}_{r_{\tau'\tau'}} = \left\{ \int_0^{\upsilon_{\max}} |r_{\tau'\tau'}(\upsilon) - \tilde{r}_{\tau'\tau'}(\upsilon)|^p \, d\upsilon \right\}^{1/p}, \tag{5.17}$$

where $p = 1, 2, ...$ and the quantity $\upsilon_{\max}$ is defined by $\upsilon_{\max} = \mathcal{L}/(2\tau_{\max})$ [26].

5.3 Mobile-to-Mobile MIMO Channel

Communication systems with a transmitter, a mobile radio channel, and a receiver can be classified by the number of inputs and outputs. The last chapters, dealing with the modeling of mobile-to-mobile propagation channels, have been described for the use of single-input single-output (SISO) systems, i.e., a single antenna at both ends of the channel, whereas the transmitter and the receiver are in motion. In this chapter, the mobile-to-mobile SISO street model is extended into the application of multiple transmit and receive antennas so-called multiple-input multiple-output (MIMO) systems.

5.3.1 Background

Multiple antennas at the transmitter and receiver are becoming very common in wireless systems. The improvements, compared to SISO systems, is not only the system performance with the high link quality, but also the capacity with higher data rates [27, 28, 29]. The advantages of MIMO communication are achieved through a relationship of antenna arrays that support spatial diversity from the propagation channel and algorithms that conform to the varying channel. Antenna arrays are developed by using antenna theory, whereas the algorithms are designed under simplified assumptions for the channel, such as fading and correlation. Therefore, the antenna geometry and the algorithm design are mostly developed separately.

In multiple-antenna systems with n_T transmit and n_R receive antennas, data is sent simultaneously from the transmit antennas. The signal received at each antenna is therefore a superposition of the n_T transmitted signals decomposed by multiple fading. Figure 5.10 shows a MIMO system with n_T transmit and n_R receive antennas. A MIMO channel is represented by an n_R x n_T matrix whose element h_{ij} ($i = 1, ..., n_R$ and $j = 1, ..., n_T$) represents the diffuse component of the channel between the jth transmit antenna and the ith receive antenna.

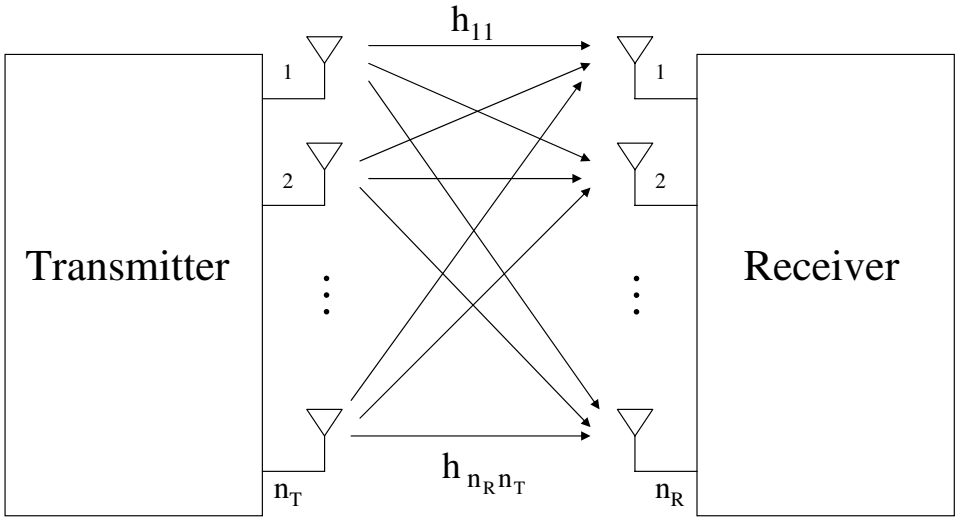

Figure 5.10: Schematic of a MIMO system with n_T transmit and n_R receive antennas

5.3.2 Geometrical Channel Model

The geometrical street model for a mobile-to-mobile MIMO channel is shown in Fig. 5.11. The transmitter and the receiver are set with two omnidirectional antennas, i.e., the design of a 2 x 2 MIMO system. The employed antennas for this configuration are, e.g., antenna arrays or multiple dipole antennas. For a reason of simplification, it is assumed that there is no line-of-sight between the transmitter and the receiver and only the frequency nonselective channel is considered.

The geometrical street model for a MIMO channel shown in Fig. 5.11 is an extension of the SISO street model in Fig. 2.1 with a space between two antennas at each mobile. The antennas at the transmitter (receiver) are represented by $A_T^{(1)}$ ($A_R^{(1)}$) and $A_T^{(2)}$ ($A_R^{(2)}$). The symbols δ_T and δ_R denote the antenna spacings at the transmitter and the receiver, respectively. The angles of spreading $\Delta\alpha$ and $\Delta\theta$ are still random variables. The scatterers are assumed to be uniformly distributed in a cluster. Furthermore, the transmitter (receiver) are on the move in the direction denoted by the angle of motion α_v (θ_v) with the speed v_T (v_R).

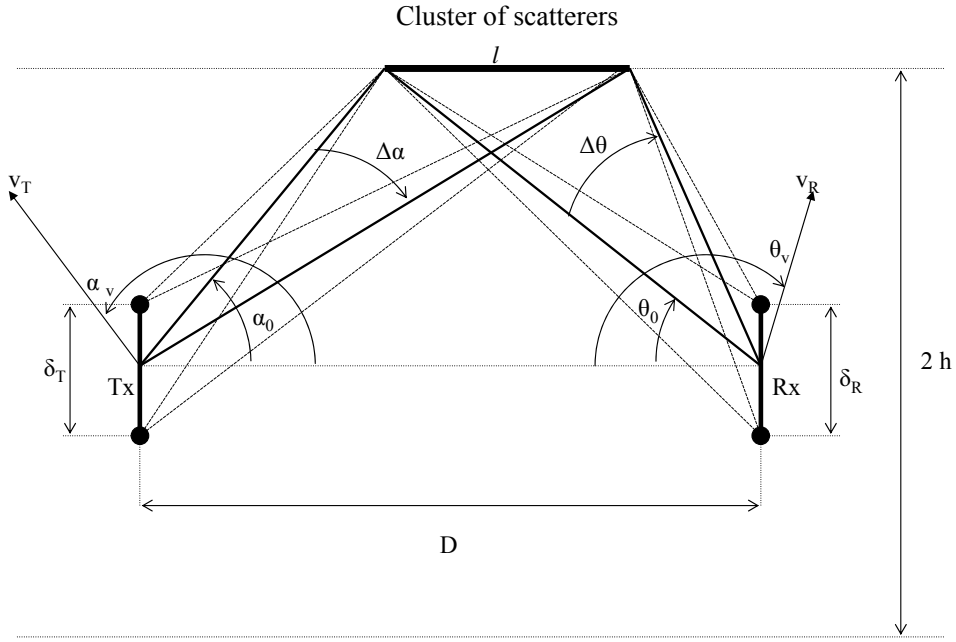

Figure 5.11: Geometrical street model for a 2 x 2 MIMO system

5.3.3 Stochastic Analytical Model

Since a 2 x 2 MIMO system is considered, the stochastic channel matrix of the components $h_{ij}(t)$ $(i, j = 1, 2)$ of the link from $A_T^{(j)}$ to $A_R^{(i)}$ is represented by

$$\mathbf{H}(t) = \begin{pmatrix} h_{11}(t) & h_{12}(t) \\ h_{21}(t) & h_{22}(t) \end{pmatrix}. \tag{5.18}$$

An important property of the MIMO channel that effectively determines the channel capacity is the correlation between the channel coefficients. It is normal to assume that the fading between a pair of transmit and receive antennas are independent and uniformly distributed random variables, when multiple antenna systems are taken into account. However, the fading in propagation environments is actually dependent because of the local scattering or too small antenna spacing [33]. In contrast, it is often necessary to use a small antenna element spacing to fit multiple antennas on a portable device, which introduces mutual coupling of the antenna elements that affects the achievable capacity of the system.

For the derivation of the analytical model, the space-time cross correlation function (CCF) between the components $h_{11}(t)$ and $h_{22}(t)$ is needed and given by

$$\rho(\delta_T, \delta_R, \tau) = E\left\{h_{ij}(t)h_{ij}^*(t+\tau)\right\}, \tag{5.19}$$

where $(\cdot)^*$ is referred to as the complex conjugation. The space-time CCF can also be expressed as a product of the correlation function between two antennas spacing concerning the transmit side $\rho_T(\delta_T, \tau)$ and the correlation function with respect to the receive side $\rho_R(\delta_R, \tau)$, i.e.:

$$\rho(\delta_T, \delta_R, \tau) = \rho_T(\delta_T, \tau) \cdot \rho_R(\delta_R, \tau), \tag{5.20}$$

where

$$\rho_T(\delta_T, \tau) = \int_0^{\Delta\alpha_{\max}} e^{-j2\pi\left[\left(\frac{\delta_T}{\lambda}\right) sin(\alpha_0 - \Delta\alpha) + f_T(\Delta\alpha)\tau\right]} p_{\Delta\alpha}(\Delta\alpha) d\Delta\alpha \tag{5.21}$$

and

$$\rho_R(\delta_R, \tau) = \int_0^{\Delta\theta_{\max}} e^{-j2\pi\left[\left(\frac{\delta_R}{\lambda}\right) sin(\theta_0 + \Delta\theta) + f_R(\Delta\theta)\tau\right]} p_{\Delta\theta}(\Delta\theta) d\Delta\theta. \tag{5.22}$$

As the quantities δ_T and δ_R define the distance between two antenna elements at the transmitter and the receiver, the spatial separation can be normalized by the wavelength λ to δ_T/λ and δ_R/λ. The probability density function of $\Delta\alpha$ and $\Delta\theta$ are defined by (3.6) and (3.7), respectively. The quantity $f_T(\Delta\alpha)$ ($f_R(\Delta\theta)$) denotes the Doppler frequency at the transmitter (receiver) and is given by (3.24). Hence, (5.21) and (5.22) will be evaluated numerically in the next subsection.

5.3.4 Numerical Results

The correlation function of the transmitter (receiver) is considered as a function of the normalized antenna spacing δ_T/λ (δ_R/λ), the delay τ, the initial angle of departure α_0 (θ_0), and the angle of spreading $\Delta\alpha$ ($\Delta\theta$). Figure 5.12 and 5.13 shows the results of the correlation at the transmitter and the receiver for $\Delta\alpha_{\max} = \Delta\theta_{\max} = 71.7^o$ with $\alpha_0 = 45^o$ and $\theta_0 = 26.6^o$ in comparison to $\Delta\alpha_{\max} = \Delta\theta_{\max} = 18.4^o$. The mobiles are in the direction of motions $\alpha_v = \theta_v = 120^o$, i.e., they are moving apart with $v_T = v_R = 50$km/h.

As it can be seen from Fig. 5.12 and 5.13, when $\Delta\alpha$ or l and $\Delta\theta$ are small, the transmit correlation and the receive correlation are high as compared to the large $\Delta\alpha$ or l and $\Delta\theta$, where the correlations are smaller.

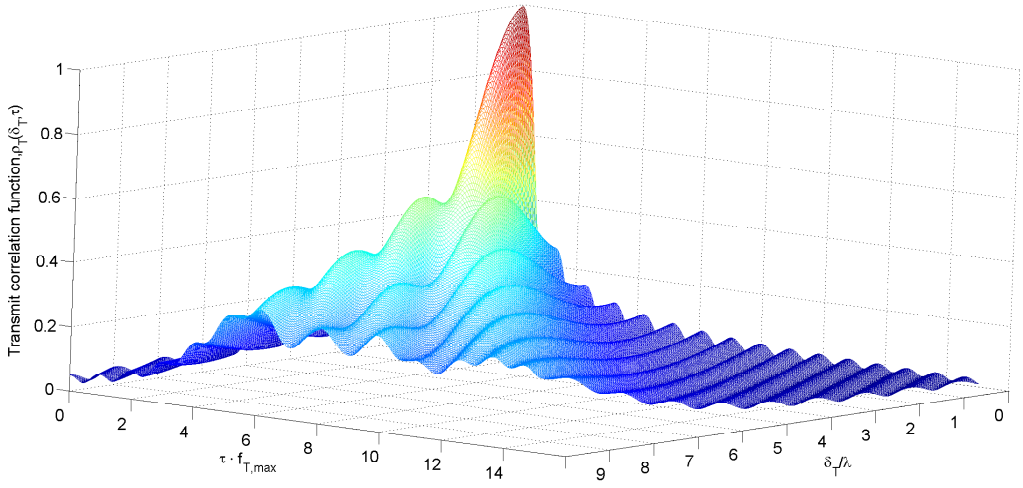

(a)

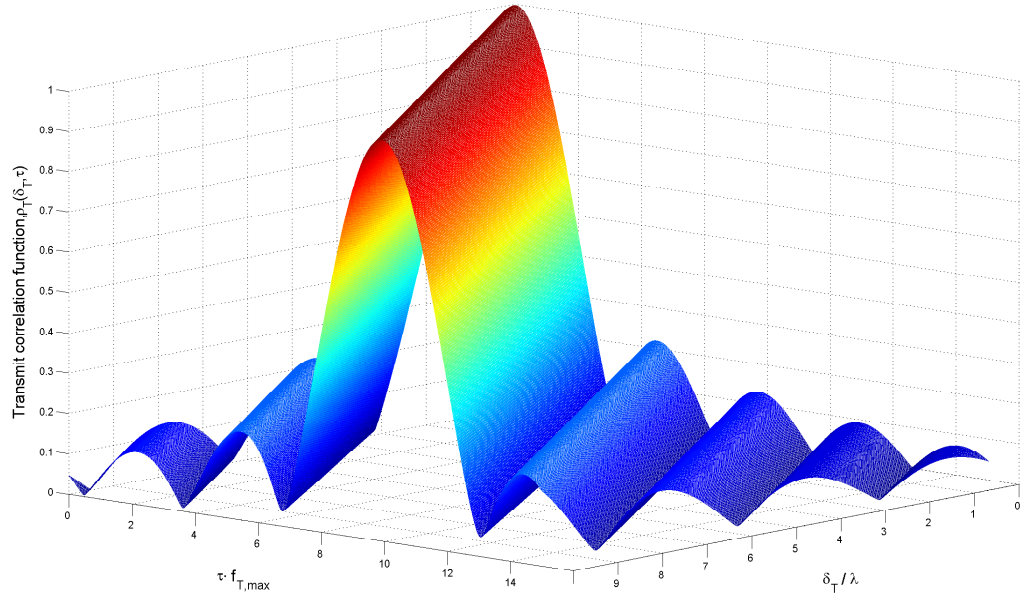

(b)

Figure 5.12: The transmit correlation function $\rho_T(\delta_T, \tau)$ of the 2x2 mobile-to-mobile MIMO channel model for (a) $\Delta\alpha_{\max} = 71.7^o (l = 15)$ and (b) $\Delta\alpha_{\max} = 18.4^o (l = 5)$

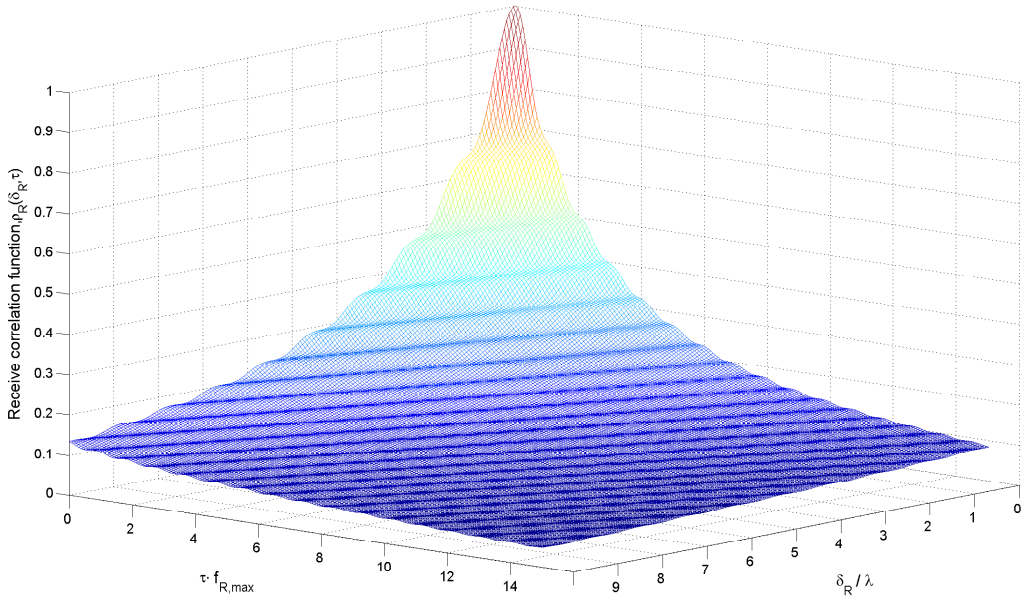

(a)

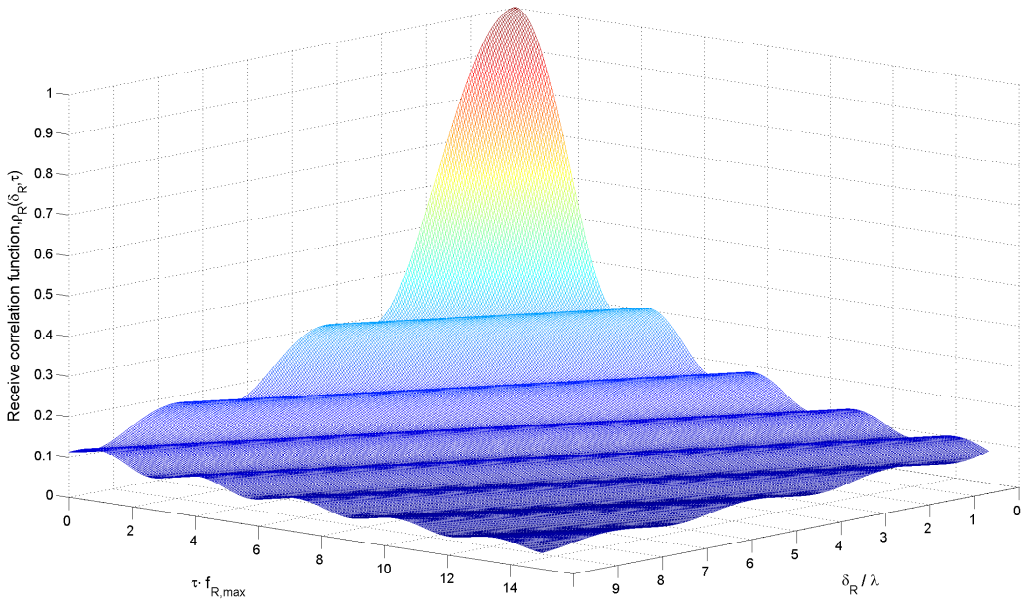

(b)

Figure 5.13: The receive correlation function $\rho_R(\delta_R, \tau)$ of the 2x2 mobile-to-mobile MIMO channel model for (a) $\Delta\alpha_{\max} = 71.7^o (l = 15)$ and (b) $\Delta\theta_{\max} = 18.4^o (l = 5)$

Furthermore, the direction of motions of the transmitter α_v and the receiver θ_v is also taken into consideration. Figure 5.14 and 5.15 illustrate the transmit and receive correlation function due to different α_v and θ_v, respectively. This indicates that the correlation function is varied, when the transmitter and the receiver move to each other, apart, or in the same direction. Figure 5.14 and 5.15 show that the transmit and receive correlation function totally depend on the θ_v and α_v, respectively.

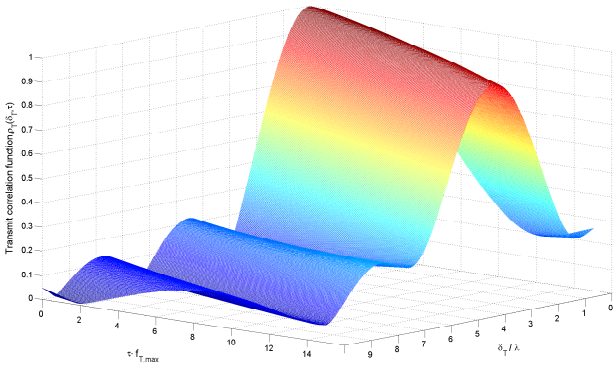

(a)

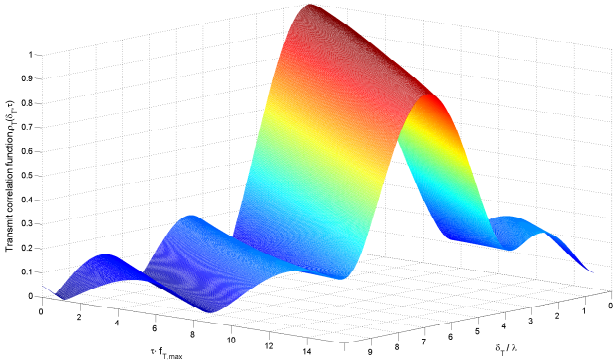

(b)

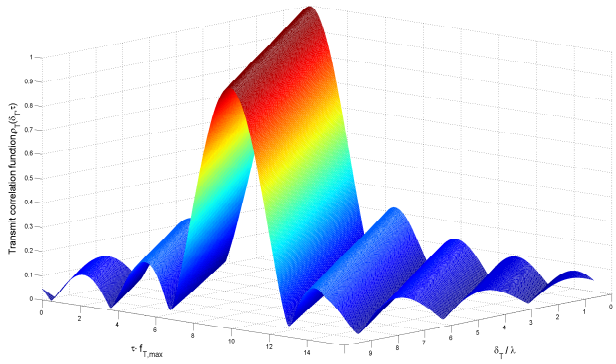

(c)

Figure 5.14: The transmit correlation function $\rho_T(\delta_T, \tau)$ of the 2x2 mobile-to-mobile MIMO channel model for (a) $\alpha_v = \theta_v = 50^o$, (b) $\alpha_v = 60^o, \theta_v = 120^o$, and (c) $\alpha_v = \theta_v = 120^o$

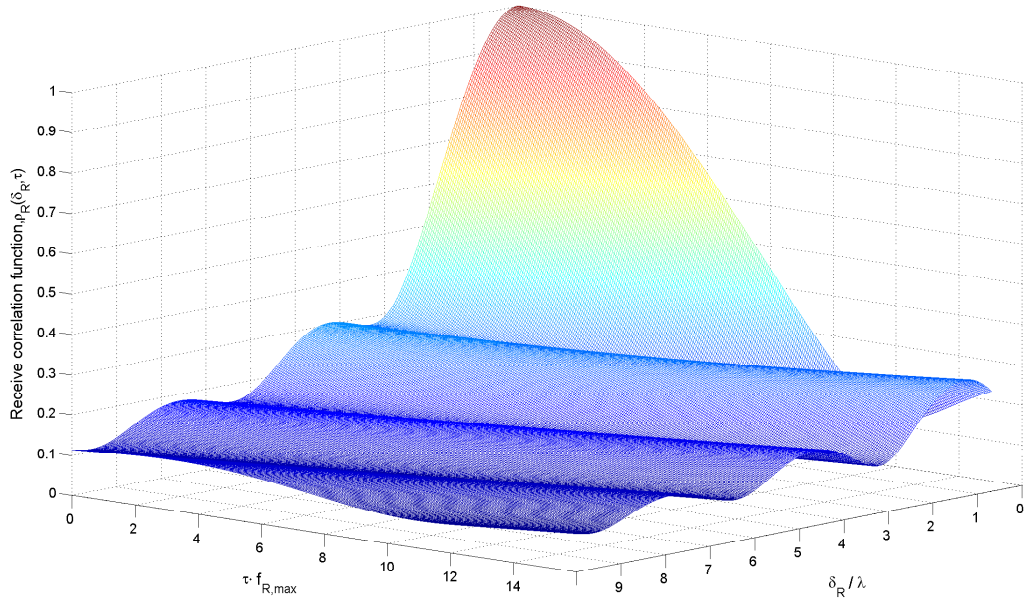

(a)

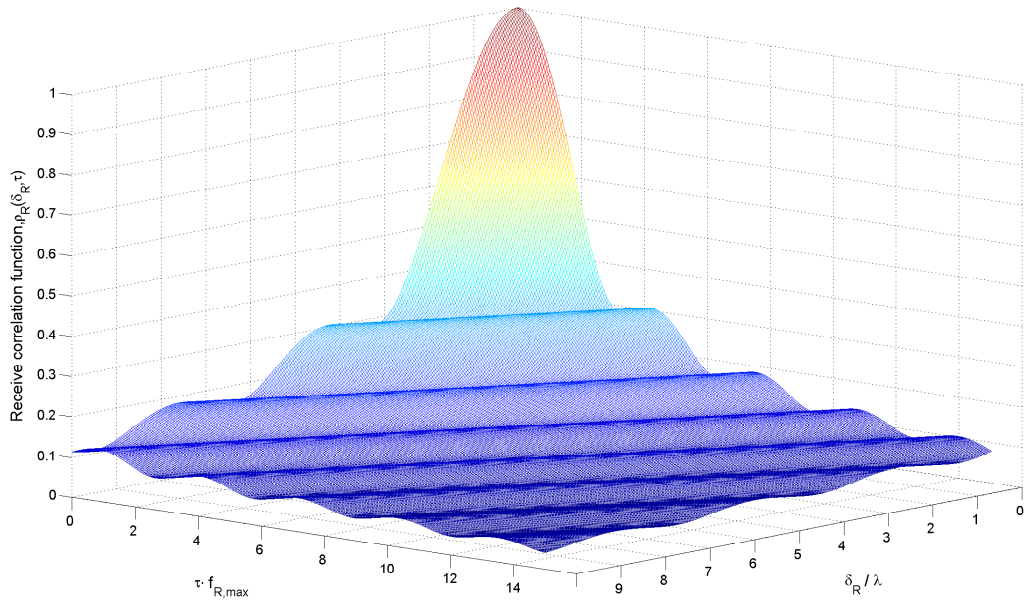

(b)

Figure 5.15: The receive correlation function $\rho_R(\delta_R, \tau)$ of the 2x2 mobile-to-mobile MIMO channel model for (a) $\alpha_v = \theta_v = 50^o$ and (b) $\alpha_v = \theta_v = 120^o$

Chapter 6

Discussions

The focus of this thesis was to model, analyze, and simulate the mobile-to-mobile MIMO channels. In this chapter, trends are presented and relationships between different parameters and the statistical properties of the channel among the results are given below.

Various relationships between the width from mobiles to the roadside h and the distance D between mobiles were evaluated in Chapter 3. It turned out that for the maximum length of a cluster, i.e., $l = D$ the most probably angular spread $\Delta\theta$ is in a very small range for small relations h/D and it increases as h/D is greater. Furthermore, the smaller a relationship between h/D, the greater the normalized PSD is, and the longer the absolute value of the ACF stays closer to one. For smaller values of h/D, the LCR is decreased, i.e., less levels are crossed, in contrast, the ADF is greatly increased. Moreover, different positions of a cluster (referred to the transmitter) has been investigated. As a result, the shorter and closer the cluster to the transmitter, the more likely a smaller the angular spread $\Delta\theta$ at the receiver is.

Moreover, the directions of motions of the mobiles influence the Doppler PSD, but no analytical solution has been computed from the PDF of the angular spread $p_{\Delta\theta}(\Delta\theta)$ due to the difficulty of the transformation of random variables. Therefore, the ACF was not calculated by the inverse Fourier transformation of the Doppler PSD. The followed alternative approach by exploiting the statistical expected value of the complex Gaussian random process led to a term of the ACF. It indicates that the more differing the direction of movement of the mobiles from each other, the steeper the ACF declines.

In Chapter 4, the simulation models were introduced. The analytical and simulation results of the PDF of the angular spread and the Doppler PSD were fit very well. In contrast, the analytical and simulation results of the ACF were not exactly identical. Neither the simulation results of the LCR nor the ADF were fit perfectly with the analytical results. Therefore, the deeper study of the LCR and the ADF of the simulation model for the mobile-to-mobile street model is needed in future work.

In Chapter 5, the performance of mobile-to-mobile MIMO street model was studied. It has been shown that the smaller $\Delta\alpha$ and $\Delta\theta$, the higher the transmit and receive correlation is. Furthermore, the transmit (receive) correlation depends strongly on the δ_T (δ_R) and τ_T (τ_R), which depends on the direction of motion α_v (θ_v). Depending on this direction, cases could be studied where only a well defined spatial separation causes a slowly decreasing CCF along its delay. According to the direction of motion, different antenna configurations are optimal.

Chapter 7

Conclusions

In this thesis, the performance of mobile-to-mobile MIMO channel was studied, which can be extended to the research on mobile Ad-hoc networks and intelligent transportation systems. A knowledge of the multipath fading channel characteristics is essential for the design of mobile-to-mobile MIMO communication systems. The development procedure of the geometrical street model was followed from the principle of deterministic channel modeling for the analytical and simulation models. The starting point of the research procedure was the geometrical street model for the application of SISO systems. Thus, the statistical properties, such as the PDF of the AOA, the Doppler PSD, the ACF, the LCR, and the ADF have been investigated. The obtained theoretical results have been confirmed by MATLAB simulations. The L_p-norm method has been applied for computation of the model parameters. Therefore, the performance of the simulation model has been evaluated by comparing its statistical properties with those of the analytical model. The geometrical street model has been extended for environments with several clusters of scatterers with respect to frequency-selectivity and finally to a MIMO street model. It has been shown that the ACF, the FCF, and the CCF can be computed independently from each other.

Extensions to the work presented in this thesis could be the study of channel capacity of the mobile-to-mobile MIMO street model and the implementation of different PDF's of the angular spreading $\Delta\alpha$ at the transmitter, such as Laplacian, Gaussian, and cosine. Moreover, the clusters could be extended in such a way that the propagated waves are affected differently by each scatterer in a cluster. Finally, the transmission could undergo multiple bounces going from the transmitter to the receiver.

Bibliography

[1] M. Pätzold, "Mobile Fading Channels", *John Wiley & Sons*, February 2002

[2] M. Pätzold, B. O. Hogstad, N. Youssef, D. Kim, "A MIMO mobile-to-mobile channel model: Part I - The reference model", *IEEE International Symposium on Personal, Indoor and Mobile Radio Communications*, September 2005

[3] M. Pätzold, B. O. Hogstad, N. Youssef, D. Kim, "A MIMO mobile-to-mobile channel model: Part II - The simulation model", *IEEE International Symposium on Personal, Indoor and Mobile Radio Communications*, September 2005

[4] G. L. Stüber, "Principles of Mobile Communication", *Springer*, December 2000

[5] M. D. Austin and G. L. Stüber, "Velocity adaptive handoff algorithms for microcellular systems", *IEEE Transactions on Vehicular Technology*, vol. 43, August 1994

[6] J. C. Liberti and T. S. Rappaport, "A geometrically based model for line-of-sight multipath radio channels", in *Proceeding IEEE Vehicular Technology Conference*, April 1996

[7] T. Fulghum and K. Molnar, "The Jakes fading model incorporating angular spread for a disk of scatterers", in *Proceeding IEEE Vehicular Technology Conference*, 1998

[8] T. Fulghum, K. Molnar, and A. Duel-Hallen, "The Jakes fading model for antenna arrays incorporating azimuth spread", *IEEE Transactions on Vehicular Technology*, vol. 51, August 2002

[9] D.-S. Shiu, G. J. Foschini, M. J. Gans, and J. M. Kahn, "Fading correlation and its effect on the capacity of multielement antenna systems", *IEEE Transactions on Communications*, vol. 48, March 2000

[10] M. Pätzold and B. O. Hogstad, "A Space-time channel simulator for MIMO channels based on the geometrical one-ring scattering model", *IEEE Vehicular Technology Conference*, vol. 1, September 2004

[11] R. B. Ertel, P. Cardieri, K. W. Sowerby, T. S. Rappaport, and J. H. Reed, "Overview of spatial channel models for antenna array communication systems", *IEEE Personal Communications*, February 1998

[12] M. Pätzold, "On the stationarity and ergodicity of fading channel simulators based on Rice's sum-of-sinusoids", *International Journal of Wireless Information Networks*, vol. 11, April 2004

[13] A. Papoulis and S. U. Pillai, "Probability, Random Variables, and Stochastic Processes", *Boston: McGraw-Hill*, 2002

[14] R. Janaswamy, "Radiowave Propagation and Smart Antennas for Wireless Communications", *Boston: Kluwer Academic Publishers*, 2001

[15] T. S. Rappaport, "Wireless Communications", 2nd Edition, *Prentice Hall*, 2002

[16] H. Wesolowski, "Mobile Communication Systems", *John Wiley & Sons*, 2002

[17] P. van Rooyen, M. Lotter, and D. van Wyk, "Space-Time Processing for CDMA Mobile Communications", *Kluwer Academic Publishers*, 2000

[18] M. Pätzold and N. Youssef, "Modelling and simulation of direction-selective and frequency-selective mobile radio channels", *International Journal of Electronics and Communications*, vol. AEÜ-55, 2001

[19] C. S. Patel, G. L. Stüber, and T. G. Pratt, "Simulation of Rayleigh faded mobile-to-mobile communication channels", in *Proceeding 58th IEEE Vehicular Technology Conference*, October 2003

[20] S. S. Mahmoud, Z. M. Hussain, and P. O'Shea, "A multipath mobile channel model for microcell environment", in *Proceeding IEEE Eighth International Symposium on Spread Spectrum Techniques and Applications*, 2004

[21] A. Goldsmith, "Wireless Communications", *Cambridge University Press*, 2005

[22] M. Pätzold, "Random variables and stochastic processes for communication engineering", *Lecture*, 2006

[23] R. H. Clarke, "A statistical theory of mobile-radio reception", *The Bell System Technical Journal*, vol. 47, July-August 1968

[24] W. C. Jakes, Ed., "Microwave Mobile Communication", *Wiley*, NY, 1974

[25] P. A. Bello, "Characterization of randomly time-variant linear channels", *IEEE Transactions on Communication Systems*, vol.11, 1963

[26] M. Pätzold and A. Szczepanski, "Methods for modeling of specified and measured multipath power delay profiles", *Proceeding IEEE Vehicular Technology Conference*, 2000

[27] J. Winters, "On the capacity of radio communication systems with diversity in a Rayleigh fading environment", *IEEE Journal on Selected Areas in Communications*, June 1987

[28] E. Telatar, "Capacity of multi-antenna Gaussian channels", *European Transactions on Telecommunications*, vol. 10, 1999

[29] G. J. Foschini and M. J. Gans, "On limits of wireless communications in a fading environment when using multiple antennas", *Wireless Personal Communications*, 1998

[30] A. S. Akki, "Statistical properties of mobile-to-mobile land communication channels", *IEEE Transactions on Vehicular Technology*, vol. 43, November 1994

[31] H. Kang, G. L. Stüber, T. G. Pratt, and M. A. Ingram, "Studies on the capacity of MIMO systems in mobile-to-mobile environment", *IEEE Transactions on Vehicular Technology*, vol. 43, November 1994

[32] B. O. Hogstad, M. Pätzold, A. Chopra, D. Kim, and K. B. Yeom, "A wideband MIMO channel simulation model based on the geometrical elliptical scattering model", in *Proceeding 15th Meeting of the Wireless World Research Forum*, December 2005

[33] B. Salz and J. H. Winters, "Effect of fading correlation on adaptive arrays in digital mobile radio", *IEEE Transactions on Vehicular Technology*, vol. 43, November 1994